BEATRIZ MIRANDA DA SILVA

MANIPULATION AND MAGNETO-MECHANICAL CONFIGURATIONS OF FLEXIBLE MAGNETIC NANODISKS

Dissertation presented to the Universidade Federal de Viçosa, in partial fulfillment of the requirements of the Physics Graduate Program, for the degree of *Magister Scientiae*.

Adviser: Vagson Luiz de Carvalho Santos

VIÇOSA - MINAS GERAIS
2022

Ficha catalográfica elaborada pela Biblioteca Central da Universidade Federal de Viçosa - Campus Viçosa

T
S586m
2022

Silva, Beatriz Miranda da, 1995-
Manipulation and magneto-mechanical configurations of flexible magnetic nanodisks / Beatriz Miranda da Silva. – Viçosa, MG, 2022.
1 dissertação eletrônica (51 f.): il. (algumas color.).

Orientador: Vagson Luiz de Carvalho Santos.
Dissertação (mestrado) - Universidade Federal de Viçosa, Departamento de Física, 2022.
Referências bibliográficas: f. 48-51.
DOI: https://doi.org/10.47328/ufvbbt.2022.490
Modo de acesso: World Wide Web.

1. Magnetismo. 2. Parabolóide. 3. Materiais nanoestruturados. I. Santos, Vagson Luiz de Carvalho, 1977-. II. Universidade Federal de Viçosa. Departamento de Física. Programa de Pós-Graduação em Física. III. Título.

CDD 22. ed. 538

Bibliotecário(a) responsável: Alice Regina Pinto Pires CRB-6/2523

BEATRIZ MIRANDA DA SILVA

MANIPULATION AND MAGNETO-MECHANICAL CONFIGURATIONS OF FLEXIBLE MAGNETIC NANODISKS

Dissertation submitted to the Physics Graduate Program of Universidade Federal de Viçosa in partial fulfillment of the requirements for the degree of *Magister Scientiae*.

APPROVED: February 25, 2022.

Assent:

Beatriz Miranda da Silva
Author

Vagson Luiz de Carvalho Santos
Adviser

Acknowledgements

If you wish your merit to be known, acknowledge that of other people

Chinese Proverb

First all, I would like to thank the laws of Nature for their existence. Without Them, I would not be here, alive and extremely grateful for studying part of them.

Now, the people.

My family is a big part of my life and without them I would be almost nothing. More explicitly, I have say that my mother Lucinda, my father Gil, my sister Bibis and my dog Lulu contributed enormously for who I am now and for what I have achieved. To be fair, I highlight the great presence of my mother during the tough process of writing my thesis. And even thought I will not cite the names because the number is too big, the other part of my family, i.e. cousins, aunts etc, deserve an acknowledge for their support.

I also dedicate the merits of this work to my friends. They offered me the comfort, the love and many moments of joy. With this set of things I could done the research with more easiness.

I would like to thank the ladies of the Department of Physics for their great companionship. Then thanks to Blue Eyes and Joselinda.

Without a health and happy brain the text you can read now would have never been written. Then, I have to say thanks to my psychologist Vanessa and my psychiatrist Amanda for their ability to make me function.

I have to recognize my research group for their expertise and usefulness in the development of my work. Therefore, I feel grateful for Nicolás, Pedro Henrique and Alisson.

Last but not least, I have to say with large letters "THANKS, ADORABLE VAGSON, FOR YOUR AMAZING SUPERVISION". Vagson's patience and willingness to cooperate with our research should be a subject of some sociological study. Thanks to him I was able to do my best. Together with this, it is imperative to say some words to the board of examiners. I appreciate your time and attention dedicated to this work.

Now, the funding agency.

Thanks to FAPEMIG for the financial support. With FAPEMIG'S scholarship, I had my work recognized and had the financial security to make it.

Abstract

MIRANDA-SILVA, Beatriz, M.Sc., Universidade Federal de Viçosa, February, 2022. **Manipulation and magneto-mechanical configurations of flexible magnetic nanodisks**. Advisor: Vagson Luiz de Carvalho Santos.

Modifying the shape and size of magnetoelectronics-based devices and soft robotics by controlling an external magnetic (or electric) field is a goal not fully achieved at the present moment. Nevertheless, the concept of shapeable magnetronics is a cornerstone in researches at the nanoscale size. This work consists of a theoretical contribution to this area of knowledge. Here, we study the effects of the mechanical, elastic, and magnetic parameters in the curvature of a surface initially set in a disk geometric configuration. The disk is free to move inside a specific transformation ranging from a hyperbolic paraboloid (saddle) to a paraboloid. We also use examples to sustain a proposed conjecture interconnecting the type of magnetization configuration (Vortex or Anti-Vortex) lying on the surface and its curvature.

Keywords: Magnetism. Paraboloid. Nanostructured materials.

Resumo

MIRANDA-SILVA, Beatriz, M.Sc., Universidade Federal de Viçosa, fevereiro de 2022. **Manipulação e configurações magneto-mecânicas de nanodiscos magnéticos flexíveis**. Orientador: Vagson Luiz de Carvalho Santos.

Modificar a forma e o tamanho de dispositivos e robótica “mole" (soft robotics) baseadas em magnetoeletrônica por meio do controle de um campo magnético (ou elétrico) externo é um objetivo não totalmente alcançado no presente momento. No entanto, o conceito de magnetrônica moldável é um dos pilares nas pesquisas em escala de nanômetros. Nós estudamos os efeitos dos parâmetros mecânicos, elásticos e magnéticos na curvatura de uma superfície inicialmente configurada em uma geometria de um disco. O disco está livre para se mover em uma transformação específica, indo de um parabolóide hiperbólico (sela) até um parabolóide. Nós também usamos exemplos para sustentar uma conjectura proposta que interconecta o tipo de configuração magnética (Vórtice or Anti-Vórtice) na superfície e a curvatura dela.

Palavras-chave: Magnetismo. Parabolóide. Materiais nanoestruturados.

Contents

1 Introduction **7**

2 Literature Review **9**
2.1 Applications . . . 9
2.2 Curvature Effects . . . 11
2.3 The Main Reference . . . 14

3 Theoretical Model **16**
3.1 The Problem and Notations . . . 16
3.2 The Building Blocks . . . 18
3.2.1 Gaussian Curvature . . . 18
3.2.2 Elastic Parameters . . . 21
3.2.3 Ferromagnetism . . . 24
3.2.4 Merons . . . 26
3.3 Magnetic Energy . . . 29
3.3.1 Anisotropy and Exchange energies . . . 29
3.3.2 Zeeman Energy . . . 30
3.4 Elastic Energy . . . 31

4 Results and Discussion **33**
4.1 Curvature-Vorticity Conjecture . . . 33
4.1.1 Main Parametrization P1 . . . 34
4.1.2 Parametrization P2 . . . 35
4.1.3 Parametrization P3 . . . 36
4.2 Exchange energy of the vortex configuration in planar and paraboloidal structures . . . 38
4.2.1 Disk . . . 39
4.2.2 Paraboloid . . . 39
4.3 Magnetoelastic quasi-2D system . . . 40
4.3.1 Radius . . . 40
4.3.2 Young's modulus . . . 42
4.3.3 Chirality and Polarity . . . 43
4.3.4 External Magnetic Field . . . 44

5 Conclusion and Perspectives **46**

Chapter 1

Introduction

> "The beginning is the most important part of the work."
>
> Plato

Traditional robots, also known as hard robots, face a common difficulty to move in environments that are not controllable or previously known, like uneven ground. Therefore, they have challenges while moving in uncertain terrains, and are susceptible to break or topple, becoming unable to move again. To change this scenario, the research in soft robotics emerged. Countless are the examples and possibilities of this kind of robot. Among several examples, one can cite robots capable of moving through controlling the air pressure and the presence of joints AirRobot, a robot made of soft-elastic materials [(1)] that mimics the movements of the octopus, and a snake-like robot[(2)],[(3)].

Although we cite a long list of applications to better motivate the readers, this is a theoretical work. We aim to captivate engineers and physicists to read this work with the ambition to use it as a reference to the description of the development of applications regarding soft magnetoelectronics. So, both hands-on people and more theoretical minds would perhaps benefit from reading this text.

In this work, we analyze the properties of a magnetoelastic disk under a specific geometrical transformation, and study its equilibrium curvature (which is, by definition, the curvature where the total energy of the system assumes its minimum value). For this purpose, we have determined the magnetic and elastic contributions to the total energy. Therefore, we analyze mechanical (elastic) and magnetic physical parameters to determine their influence on the optimum curvature of a nanodisk hosting a meron as a metastable state. In this context, we have analyzed a conjecture concerning Gaussian curvature and meron's winding number, as previously discussed by Elías *et al.*(4). Additionally, we obtain the relationship between the surface's curvature and the meron's winding number by using two possible geometrical transformations describing surfaces that change their curvatures from negative to positive. As a result, we obtain the relationship between the surface's curvature and the meron's winding number.

Now, we present the path the reader will encounter while reading this thesis. The first chapter is called "Literature Review" (ch. 2) and concerns, as its name suggests, to a brief review of correlated papers about curvature effects on the magnetic

and mechanical properties of flexible and rigid systems. The second chapter is the “Theoretical Model" (ch.3), where we present the specific geometrical description of the considered system in which we based our main results relating curvature and magneto-elastic effects. It is also introduced the essential concepts like the magnetic configurations we consider and definitions like meron’s polarity of the core p, chirality γ, and the winding number q. We also present the notions of magnetic energy, given by anisotropy and exchange energies. Additionally, we present the expressions for the elastic energy, including the stretching and the bending terms.

Following the “Theoretical Model", we present the main contribution of this work, which is the chapter “Results and Discussion" (ch. 4). There, we analyze the behavior of the curvature and the energy as a function of several parameters, such as the disk’s external radius, the thickness of the disk, the Young’s modulus, the vortex chirality-polarity, and external magnetic field.

Finally, we finish this text with the chapter “Conclusions and Perspectives" (ch. 5), which presents the main conclusions on the obtained results, and our prospects for future works.

Chapter 2

Literature Review

> "You're unlikely to discover something new without a lot of practice on old stuff, but further, you should get a heck of a lot of fun out of working out funny relations and interesting things."
>
> Richard P. Feynman

This thesis concerns the application of the theory of ferromagnetism and elasticity to investigate a problem of a magnetic quasi-2D system varying in shape and size. Therefore, it is opportune to begin this chapter by giving the motivation and the general facts relating directly or indirectly with our work. We divided this chapter into three sections: "Applications" (sec. 2.1), to give the reader a glimpse of the more practical aspects of flexible magnetism, "Curvature Effects" (sec. 2.2) to present important some results regarding curvature and magnetic systems, and "The Main Reference"(sec. 2.3), which presents the paper from which we decided to reproduce and extend their results.

2.1 Applications

The concept of flexible and stretchable electronics is a very prominent topic. With this concept, the old notion of electronic devices as being hard and of a fixed form is no longer true. Examples of this kind of research is available to sensory devices [5; 6; 7], solar cells[8], electronic skins [5; 9; 10; 11], soft robotics [12], and wearable devices[13], just to cite some of them. A very nice possibility on this issue is the inclusion of a magnetic degree of freedom into these soft systems. With this new aspect, one is able to manipulate the shape and geometry of the magnetic soft system by using an external magnetic field. One example of this topic can be found in the emerging field of soft robotics and even in actuators which have variable shape [14].

The main goal of the concept of shapeable magnetoelectronics is to promote rigid devices into their shapeable counterparts, as stated in Markarov *et al.*[14]. Here, "shapeable" should be understood as flexible, printable and stretchable. One can see in

Fig. 2.1 some of the promising products and prototypes that can be done by using the notion of flexibility in usual rigid magnetoelectronic devices. Amongst the presented devices, one can highlight some examples such as electronic skins, subject to compression and extension; functional implants; soft robotics, where it is visible the adaptability of this kind of robots to delicate objects.

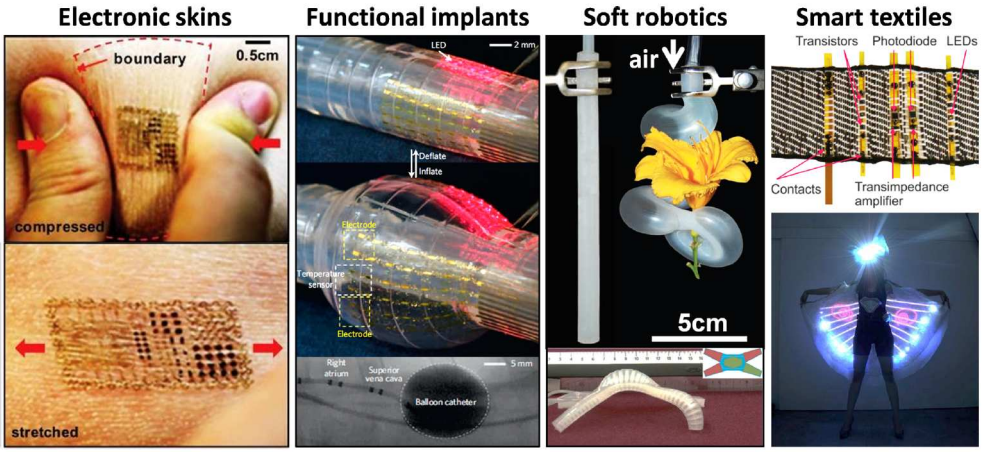

Figure 2.1: Figure extracted from (14). It is possible to see many kinds of shapeable devices, such as electronic skins, functional implants, soft robotics and smart textiles.

In many cases, materials controlled by fields and having magnetically switchable properties are made by elastomers, such as natural rubber and silicons. They consist of a non-magnetizable polymer matrix containing magnetic nanoparticles[15]. The description of the magnetic properties of such elastomers is done by considering the dipole-dipole interaction, once the intrinsic properties of the magnetic particles are independent from each other[16]. Therefore, the application of an external magnetic field induces a particle rearrangement, which is responsible for changes in the mechanical properties of the elastomer matrix[17]. Subsequently, the final and stable shape of the magnetic elastomer is influenced by the external field and the initial arrangement of the magnetic nanoparticles[18]. Therefore, the competition between magnetic interactions and the energetic cost to produce bendings and stretchings in a flexible system can make the membrane to expand, contract, or twist, in such a way that one can get many shapes as a function of the external magnetic field[19],[20].

However, the imbibition of magnetic nanoparticles in an elastic matrix avoids the possibility of leading with flexible magnetic systems at the nanoscale range of sizes. This is a problem with a solution. One can construct systems where the role is played by the short-range exchange interaction. There are many examples of systems that can be described from short-range magnetic interactions. For instance, one can cite organic, organic-inorganic hybrid, and molecular based magnets[21; 22; 23; 24]. Hence, due to the short-range nature of the exchange interaction, it is possible to reduce the size of the flexible ferromagnetic system.

2.2 Curvature Effects

When we consider the influence of the geometry on the magnetic properties of systems at the nanoscale range, it is known that the introduction of curvature in quasi-2D systems induces effective interactions[25] that are responsible for a curvature-driven polarity-chirality for vortices[26] and skyrmions[27],[28] lying in curved systems. Additionally, these effective interactions yield a curvature-induced selection on the domain wall phase[29; 30; 31], and the nucleation of a vortex/anti-vortex pair in toroidal nanoshells[32].

From the viewpoint of flexible magnetic systems, Yershov *et al.*[25] showed that the Dzyaloshinskii-Morya interaction (DMI) [1] induces spontaneous deformation of flexible ferromagnetic ribbons. The authors distinguished the DMI into two types: DMI of Bloch type, since it results in domain walls of Block type, and DMI of Nèel type. The pictorial representation of both types of domain walls are shown in Fig.2.2, where we present domain walls of the Bloch (a) and Nèel type (b).

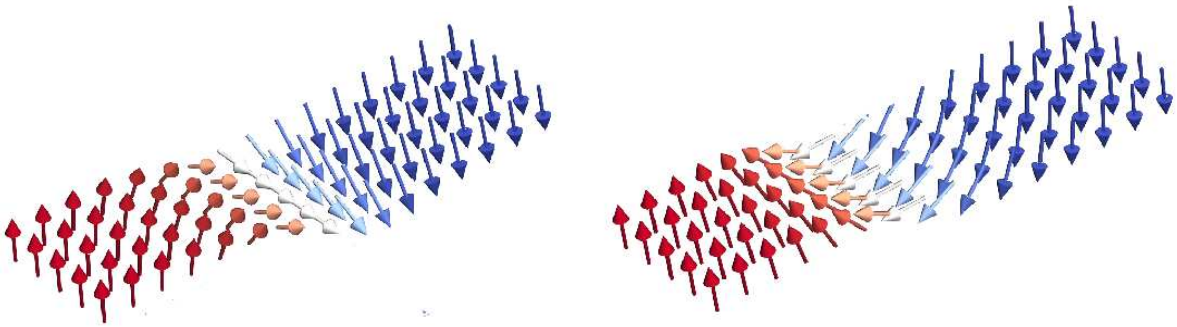

(a) Bloch Wall (b) Nèel Wall

Figure 2.2: Figure extracted from (33) with adaptations. Material with perpendicular magnetization, upper figure shows (a) the Bloch configuration and (b) the Nèel configuration

In their work, Yershov *et al.*[25] presented analytical and numerical calculations describing the equilibrium shape of the flexible nanostripes. The authors concluded that the type of DMI (Block or Néel) and the equilibrium magnetization of the stripe determines the geometrical aspects of the deformation. The authors have shown that there are three geometrical phases that the stripe can assume, so-called: the DNA-like deformation (it has a stripe central line in the form of a helix), the helicoid deformation (it has a straight central line), and the cylindrical deformation (See Fig. 2.3).

[1] An effect that privileges the perpendicular orientation of neighbors magnetic moments.

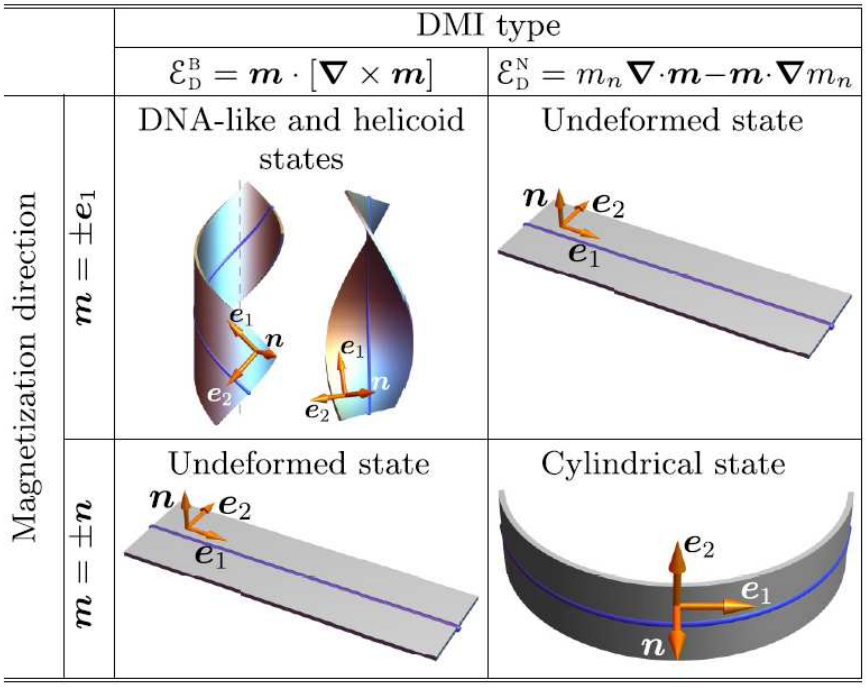

Figure 2.3: Figure extracted from (25). It is shown the possible DMI-induced deformations of flexible ferromagnetic ribbons for the Block and Néel type of DMI for two directions of magnetization

Curvature is also important to determine the properties of rigid ferromagnetic structures. For instance, Gaididei *et al* (26) have shown a mechanism to control the switching of the magnetic vortex chirality. The analyzed problem consists of a curvilinear magnetic nanoshells of spherical geometry hosting a vortex as the magnetization ground state. It is possible to control the vortex chirality by applying a Gaussian pulse [2] of spatially uniform magnetic field in the direction of the symmetry axis of the shell. The authors have numerically explored many parameters of the magnetic pulse that influences the vortex chirality switching process. Fig.2.4 shows the spherical geometry with the magnetization before (a) and after (b) the application of a simple spatially uniform pulse of magnetic field. Their main conclusion is that there is a connection between the vortex chirality and polarity, which are responsible for different switching mechanisms of the vortex core.

[2] Pulse in which its graph of intensity versus time has the shape of a Gaussian function.

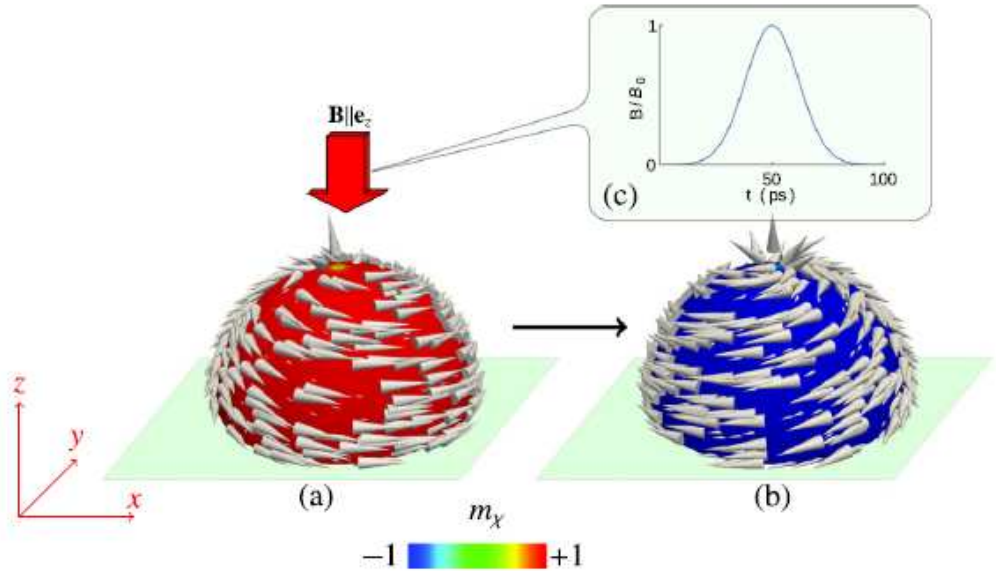

Figure 2.4: Figure extracted from (26). The image shows the vortex chirality switching for a hemisferical shell.(a) it is presented the initial vortex state with chirality $\gamma = 1$ (b) resulting vortex state with negative chirality $\gamma = -1$ (c) Gaussian temporal profile of a spatially uniform magnetic pulse.

One of the great properties of nanostructures comes from the effects generated for the curvature of the structure[28]. For instance, the physical problem investigated by Carvalho-Santos *et al.*[28] was the influence of the geometry on the skyrmion stability in a ferromagnetic material (FM) with thickness t deposited on top of a curved heavy metal (HM) substrate, as shown in Fig. 2.5. Amongst the main findings of the authors, one can highlight the increase of skyrmion stability due to the exchange-driven curvature induced by DMI as a function of the zenith angle ϑ for three values of the length parameter a. As the parameter a increases, the exchange-driven curvature also increases. The inverse behavior is found on the graph Fig. 2.6-a of the effective anisotropy as a function of ϑ. I.e., the anisotropy decreases with higher values of a. To resume these results, one can state that the curvature increases the effective DMI of the dome structure and decreases the effective anisotropy. Therefore, positive curvature in nanostructures enhances the skyrmion stability.

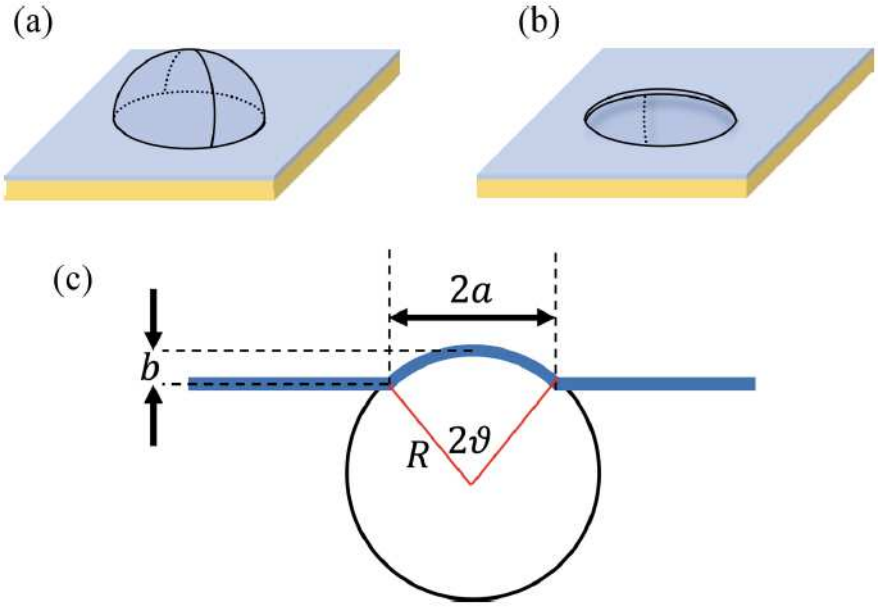

Figure 2.5: Figure extracted from (28). (a) Dome, (b) Anti-dome, (c) Definitions of the geometrical parameters

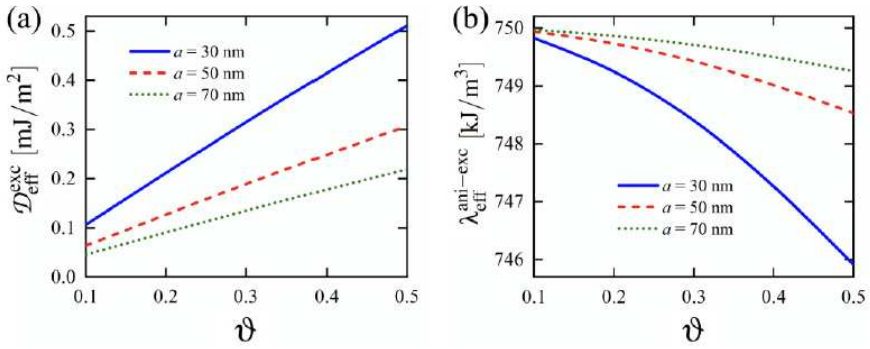

Figure 2.6: Figure extracted from (28). (a) Exchange-driven curvature-induced by DMI, (b) effective anisotropy as a function of zenith angle for three values of the geometrical parameter a. [The zenith angle ϑ and a are defined by Fig.2.5

2.3 The Main Reference

Finally, we present here the results obtained by Elías *et al.*[4], where it is shown the existence of curvature-induced winding number selection of merons hosted in a rigid curved magnetic surface. In this case, the vortex (V) is the preferable configuration of the positive Gaussian surface [3] while the anti-vortex (AV) is the minimum energy meron-like configuration in surfaces with negative Gaussian curvatures. Figure 2.7a shows the exchange energy as a function of the meron's chilarity (the angle between the magnetization of the meron and the radial vector of the surface), it is worth noticing that for a paraboloid surface the hosted merons are vortices, independent of the

[3] A Gaussian curvature, which will be further explained later on in the text, is a measure of how much the surface differs from a plane.

vortex core polarity, represented by $p = 1$ (magnetization pointing parallel to the normal vector) and $p = -1$ (magnetization pointing in the opposite direction to the normal vector). In Fig. 2.7b the anti-vortex is the metastable state also independent of the polarity. Therefore, one can conclude that the surface's geometry determines the topological properties of the metastable states.

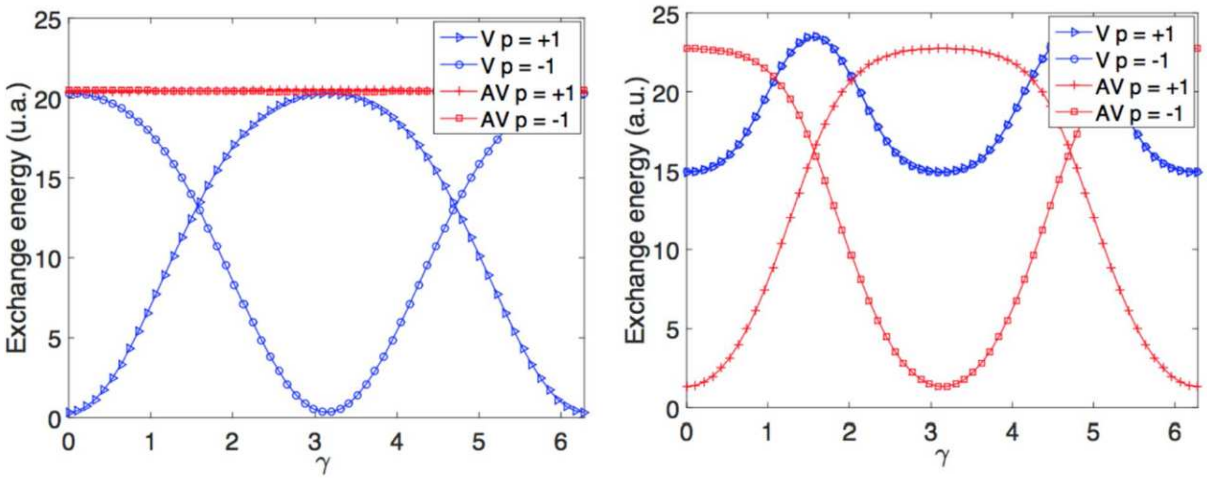

(a) Paraboloid (b) Hyperbolic Paraboloid

Figure 2.7: Figure extracted with modification from (4). Exchange energy as a function of the chirality for a) a paraboloid (positive Gaussian curvature), b) a hyperbolic paraboloid (negative Gaussian curvature) .

After, in this work, the reader will see that the results here obtained are in agreement with the results obtained by Elías *et al.*(4). Also, we present an extra freedom degree to the model, by expanding the treatment to finite flexible quasi-2D structure, where the energetic cost [4] to deform the nanostructure, represented by the elastic energy, becomes considerable if compared with the magnetic energy.

[4] In this work, energetic cost refers to the difference between the energy of the planar structure and the energy of the deformed system.

Chapter 3

Theoretical Model

> "No physical theory is worth much if it cannot be explained to a barmaid."
>
> Ernest Rutherford

In this section we present the adopted theoretical model to determine the energy contributions to describe the interplay between magnetic and elastic properties of a flexible magnetic nanodisk. The mechanical freedom degree is determined from the calculation of the elastic energy, composed by the stretching and bending terms. The magnetic energy is given by the sum between exchange and an effective anisotropy, which can be used as an approximation to determine the dipolar interaction [34]. Additionally, we decided to present interpretations of the equations, instead of the more formal approach to deduce the equation from some assumptions and approximations. For more details on the derivation of the presented equations, we suggest the references cited in this chapter.

Most of the obtained results in this work are based on numerical calculations. The reason for that are the cumbersome equations, impossible to treat without using numerical methods. Nevertheless, we have also obtained some analytical results to describe the static properties of the considered system. We use the Julia language to obtain the numerical results, and Mathematica software to compose the pictures presented in the nanomagnetic quasi-2D system. The calculation of the elastic energy was done by using the theoretical model developed by Efrati *et al.*[35], while for the magnetic energy we have used the model presented in the work of Elías *et al.* [4].

3.1 The Problem and Notations

Firstly, we define and present the general terms that we use to describe the analyzed system. We define a geometrical description considering a surface transformation going from a hyperbolic paraboloid to a paraboloid passing through a disk. The transformation is made upon a quasi-2D system, i.e., a body in which its thickness is much smaller than the other dimensions (width and height). Since the geometry of the considered system changes due the deformation, the Gaussian curvature also changes. Our main goal is to investigate what geometry the quasi-2D system reaches

as a function of the magnetization configuration, considered as a meron profile. For this purpose, we adopt the concept of optimum curvature c^*, which consists of the curvature that minimizes the total energy of the system.

We assume that the disk can only be deformed into the following transformation:

$$\vec{r} = (x, y, c^2x^2 + c|c|y^2) \tag{3.1}$$

where $x = \rho\cos\theta$, $y = \rho\sin\theta$ are the rectangular coordinates. And $\rho \in [0, R]$ and $\theta \in [0, 2\pi)$ are the curvilinear coordinates.

Additionally, $c \in [-\infty, \infty]$ is a parameter that accounts to determine the shape of the considered system. To illustrate the problem, in Fig. 3.1, we present three geometries obtained from the parametrization given in eq. (3.1) for a the quasi-2D system hosting a vortex as the magnetization vector field (the magnetic part will be explained later on the text). From left to right, we present the geometries for curvature parameter $c = 2 \times 10^3$ m$^{-1/2}$ (paraboloid), $c = 0$ (disk), and $c = -2 \times 10^3$ m$^{-1/2}$ (hyperbolic paraboloid).

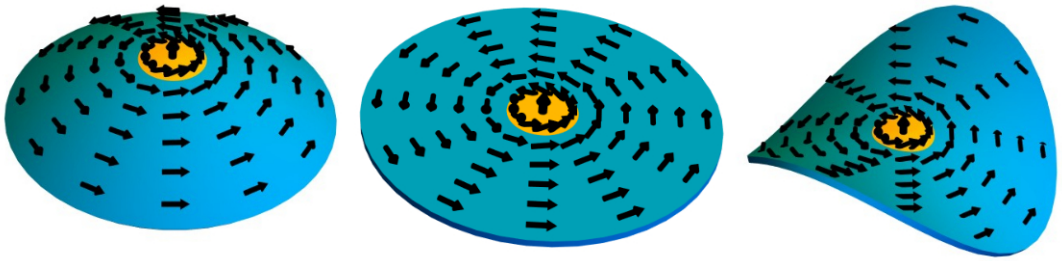

Figure 3.1: Schematic representation of the considered geometry geometrical description of the possible shapes of the considered system as a function of the parameter c. From left to right, we present the geometries for $c = 2 \times 10^3$ m$^{-1/2}$, 0, and -2×10^3 m$^{-1/2}$. The presented vector field consists of a vortex configuration, and yellow region determines the vortex core size.

Following the transformation given in the eq. (3.1), we are able to compute and set notation to the tensors we use. Firstly, we present the covariant tensor, here denoted as $g^\star$, and formally defined as the matrix:

$$g^\star = \begin{bmatrix} \frac{\partial\vec{r}}{\partial x}\cdot\frac{\partial\vec{r}}{\partial x} & \frac{\partial\vec{r}}{\partial x}\cdot\frac{\partial\vec{r}}{\partial y} \\ \frac{\partial\vec{r}}{\partial y}\cdot\frac{\partial\vec{r}}{\partial x} & \frac{\partial\vec{r}}{\partial y}\cdot\frac{\partial\vec{r}}{\partial y} \end{bmatrix} \tag{3.2}$$

The elements of the covariant tensor are denoted as g^{ij}. For example $g^{11} = \partial_x(x, y, c^2x^2 + c|c|y^2)) \cdot \partial_x(x, y, c^2x^2 + c|c|y^2)) = (1, 0, 2c^2x) \cdot (1, 0, 2c^2x) = 1 + 4c^4x^2$ in the specific transformation given in eq. (3.1). It is worth noticing that because we are adopting an approximation valid for quasi-2D systems[35], the covariant tensor is a matrix of second order and not third order.

The other very important notion is called the contravariant tensor, here symbolized by $g_\star$. The expression of g_* is determined from the relation $g^\star g_\star = I_2$, where I_2 is the identity matrix of second order. Therefore, the contravariant tensor is formally written as:

$$g_\star = \frac{1}{|g^\star|}\begin{bmatrix} g^{22} & -g^{12} \\ -g^{12} & g^{11} \end{bmatrix} \tag{3.3}$$

where, $|g^{\star}| = \sqrt{g^{11}g^{22} - (g^{12})^2}$ is the determinant of the covariant tensor. Here, we denote the elements of the matrix g_* as g_{ij}.

3.2 The Building Blocks

When asked by a layman interviewer why magnets work the way they work, the physicist Richard Feynman was puzzled. The reason was, in Feynman's own words "When you ask why something happens, how does a person answer why something happens?". Feynman patiently explained with several examples the degrees of answers in the why type of question. The reason to cite this passage is to explain here that "why"-questions should be answered in our context by going back to the concepts given as axioms (or fundamental blocks from which facts come from) in this chapter. Our goal here is to give to the reader familiarity with those axioms in order to satisfy future questions with answers that remote to this chapter.

3.2.1 Gaussian Curvature

In this subsection we have the intention to give some familiarity with the notion of Gaussian curvature to to the reader. Nevertheless, before discussing this concept in the general context of curved surfaces, we start this subsection by defining curves within a plane (plane curves). Every plane curve can be described by a parametrization $P(t) = (x(t), y(t))$ [1]. The collection of points $P(t)$ with t in an interval I gives the image of the curve. There are several examples of difficult-to-treat curves, but the discussion on such a kind of structures is out of the scope of this work. To define the concept of plane curve in a way to treat it with the tools of Differential Geometry, we consider the possibility to travel thought the curve with constant speed (greater than zero). Fig. 3.2-a shows a possible curve with could treat with the smooth assumption [2] we made, while Fig. 3.2-b presents a cusp in the origin, and therefore, they do not satisfy the condition of traveling with a constant velocity through them.

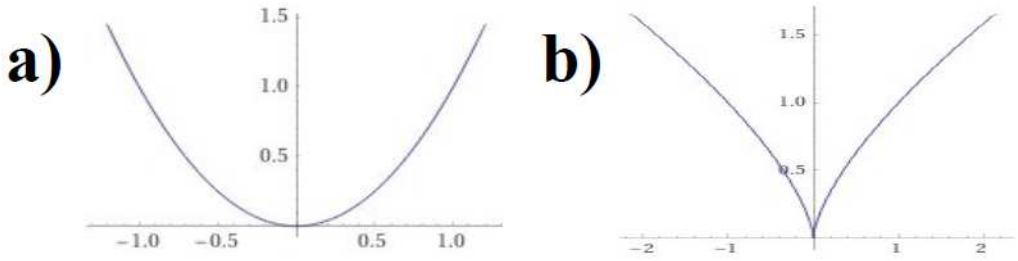

Figure 3.2: Examples of a) regular curve $P(t) = (t, t^2)$, b) irregular curve $P(t) = (t^3, t^2)$

With this consideration, we can well-define the concept of curvature in plane-curves. Fig. 3.3 shows an example of smooth curve C. Let Δs be the distance (in the curve C) between the points M and $M1$. And let $\Delta\Phi$ denote the angle between the tangent in M (red arrow) and the tangent in M_1 (purple arrow). We can define the curvature of the plane-curve c between the points M and M_1 as $K = \Delta\Phi/\Delta s$. If we

[1] x and y are the curvilinear coordinates written as a function of a parameter t.
[2] Assumption that the surface could be expressed by a function of class C^2.

take the limit in which the length Δs tends to zero, then we have the curvature in the point M.

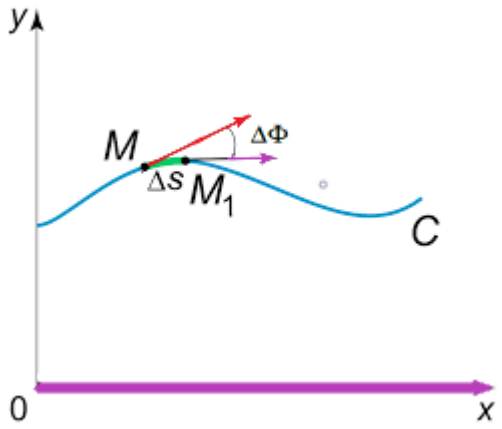

Figure 3.3: An example of a plane curve.

There is a very interesting theorem valid for plane curves, but not valid for all curves in space. It is called “Fundamental Theorem of Plane Curves", which states the following: “Two unit-speed plane curves which have the same curvature differ only by a Euclidean motion."[(36)]. The term “two unit-speed curves" is used for describing smooth curvatures in which their velocity moduli are constant (and equal to one). We can translate the theorem in simple words. Consider an initial plane curve C and whose curvature is known, without any other information about the curve. With this information, one could construct a curve identical to C, changing only the position and rotation of the curve in the plane.

Curves in space are a bit more complicated and we need additional information to reconstruct it starting from the curvature. With the plane-curves in mind, we present now the notion of Gaussian curvature of surfaces. Fig. 3.4 shows three surfaces: a hyperbolic paraboloid, a cylinder, and a sphere, which have negative, zero, and positive Gaussian curvature, respectively. To understand the notion of curvature of surfaces we have to consider two (perpendicular) lines tangent to the surfaces. In Fig. 3.4 these directions are represented as green and orange curves. If one of these curves is straight, the Gaussian curvature is zero. If both curves are not straight, then the sign of the Gaussian curvature depends on the relation between one curve to the other. For example, in Fig. 3.4a the orange curve points inside the page, while the green one points outside the page. This feature makes the Gaussian curvature of the hyperbolic paraboloid negative in all points of this surface. In the case of a sphere (See Fig. 3.4c), both curves have their curvature pointing inside the page and then, the sphere’s Gaussian curvature is positive.

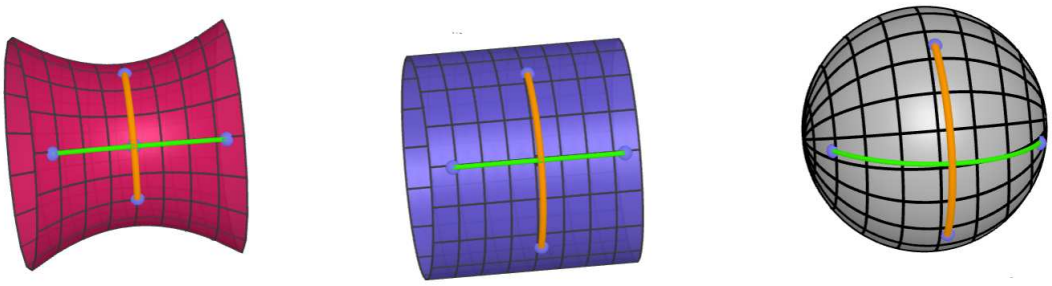

(a) A saddle. (b) A cylinder. (c) A sphere.

Figure 3.4: In Fig. a the external directions (in green and orange) curve in opposite directions, therefore the Gaussian curvature is negative. In Fig. b the Gaussian curvature is zero, then there is at least one external direction with zero curvature. Finally, in Fig. c the external directions curve in the same directions, characterizing a positive Gaussian curvature.

An important theorem was proven by Gauss concerns a crucial property of Gaussian curvature. This theorem is so meaningful that is called “Theorema Egregium", a name coming from Latin meaning “Remarkable Theorem". It says the following: “Just with the measures of distances and angles in a surface, one can determine its Gaussian curvature (independently of how the surface is embedded in space)" [37]. A corollary of this theorem is that if one bends a surface without stretching it (like bending a plane into a cylinder) the curvature remains constant. Therefore, once can conclude that two curvatures with the same value can have different shapes. For example, the plane have zero curvature, but the cylinder also have zero Gaussian curvature.

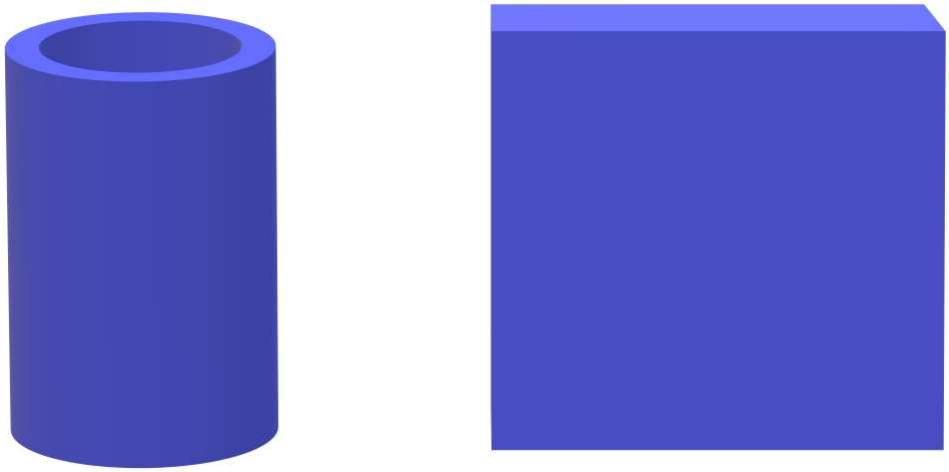

Figure 3.5: A cylinder and a plane (with thickness). Both shapes have zero Gaussian curvature.

The Gaussian curvature for surfaces parameterized by $\vec{r} = (x, y, F(x, y))$ with the function $F(x, y)$ possessing second-order derivatives, is given by:

$$K(x,y) = \frac{F_{xx}(x,y) \cdot F_{yy}(x,y) - F_{xy}^2(x,y)}{(1 + F_x^2(x,y) + F_y^2(x,y))^2} \tag{3.4}$$

Where F_{ij} denotes the second order derivative:

$$\frac{\partial^2 F}{\partial j \partial i}$$

Using the parametrization given in eq. (3.1), describing the set of geometries considered in this work, $F(x,y) = c^2x^2 + c|c|y^2$ as an example for the Gaussian curvature calculation, we have $F_{xx} = 2c^2$, $F_{yy} = 2c|c|$ and $F_{xy} = 0$. Therefore, from eq. (3.4), we obtain:

$$K(x,y) = \frac{4c^3|c|}{(1 + 4c^4(x^2 + y^2))^2} \tag{3.5}$$

From (3.5), we observe that the Gaussian curvature is not constant on the surface, because it is a function of the variables x and y. However, we are not interest in the value of K. Instead we want to analyze its sign. For the Gaussian curvature of the surface under analysis, we have an interesting result:

$$K(x,y)_{\pm} = c_{\pm} \tag{3.6}$$

where the sign ($\pm$) regards to $c > 0$ (+) and $c < 0$ (-). Therefore, in eq. (3.6), we use a notation that indicates that the magnitudes of $K(x,y)$ and c have the same sign ($K(x,y) \cdot c \geq 0$). So, from now on, instead of working with the Gaussian curvature, we use the parameter "c", referring to it as the curvature.

3.2.2 Elastic Parameters

In this subsection, we give the notions of the Poisson's ratio and the Young's modulus. To understand the concept of Poisson's ratio, let's take the example of a rubber band, as illustrated in Fig. 3.6. It is initially set in a equilibrium position presenting an initial height y_0 and a length x_0. If we apply a certain force of modulus F in a way to stretch the rubber band, the length increase by an amount Δx, and the height decrease by $-\Delta y$. It is to say, as the band is stretched, it also becomes thinner.

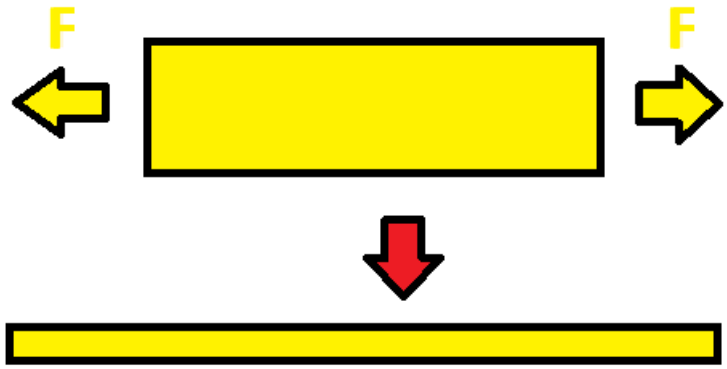

Figure 3.6: Example of a rubber band under with its extremes under the action of forces F.

In a more generic situation, let's imagine a cuboid (of dimensions x,y and z). If we compress it in the direction of $\vec{x}$ (similarly to what we did with the rubber band, but change the direction of the force), we would have a decrease $-\Delta x$ in the x-axis direction and an increase in the other dimensions.

For a quantification of how much the lateral directions deform, it was created the concept (and physical definition) called Poisson's ratio. This concept can be better understood from taking the example of the cuboid of dimensions x, y and z. Let $\vec{x}$ be the perpendicular direction, i.e., the direction where the external forces are being applied. To account the changes in these directions, we define the strains $\epsilon_i = \Delta i/i$, where i can be any of the dimensions x, y and z. It is an experimental fact that the lateral strains are equal $\epsilon_y = \epsilon_z$.[38] Moreover, they are proportional to the perpendicular strain ϵ_x [38]. The adimensional constant that links the lateral strains to the perpendicular one is called Poisson's ratio, here denoted by the greek letter ν. As the reader may imagine, this constant changes with the material. In this context, we have that

$$\nu = -\frac{\epsilon_y}{\epsilon_x} \tag{3.7}$$

After giving the physical intuition on the Poisson's ratio, we now quantify some physical parameters. First, we are dealing with isotropic materials, i.e., the physical properties are the same in all directions. Second, we are dealing with the elastic materials (i.e., materials that recover their original shapes after the external force vanishes) in its elastic regime (the linear regime in Fig. 3.8). Things can get really complicated when we surpass this regime. And third, the considered materials have a positive ν. There are materials, like cork, in which $\nu = 0$, and there are even counter-intuitive materials with negative Poisson's ratio called auxetic materials, which increase their transverse dimension when subjected to an axial tensile load[39]. The last cited materials are artificial and do not occur naturally. Therefore, it is interesting to say that the Poisson's ratio, in principle, could have any value. Actually, there is a theoretical Poisson's ratio range going from -1 to 0.5, and most of materials are restrict to the

interval $I = [0.25, 0.35]$ [40]. Additionally, several metals have a defined $\nu = 0.3$ [41], and this is the value we use in this work.

Another important mechanical characteristic of materials is the Young's modulus, which is a very useful quantity to describe how a certain material deform under two opposite external forces. To describe it, we use the tensile test mechanism depicted in Fig. 3.7. The material whose mechanical characteristics are being measured is represented in Yellow and a force being applied in its ends in a uni-axial direction (the same as the body-longest dimension). The main goal in this measure is to extract the stress *vs* strain graph until the material breaks due to the external forces.

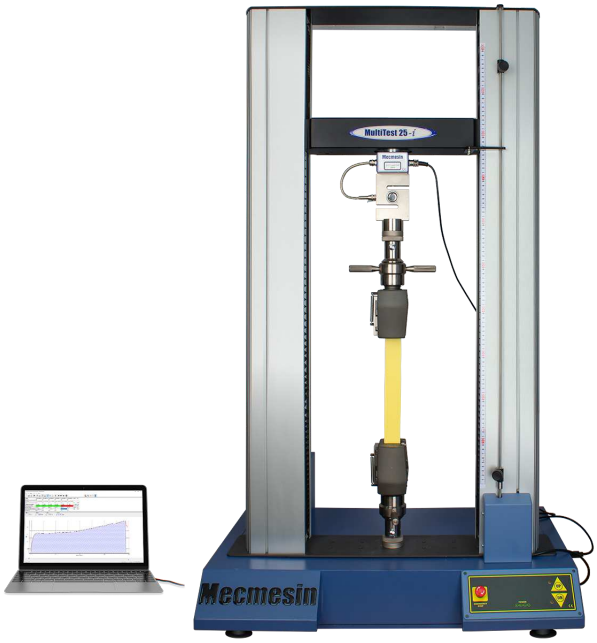

Figure 3.7: The tensile test mechanism.

The result of the stress *vs* strain graph for a typical elastic material can be observed in Fig.3.8. Initially, we see a linear dependence on the strain ϵ, which is a strong motivation to define a quantity to represent the slop of this line, called the Young's modulus.

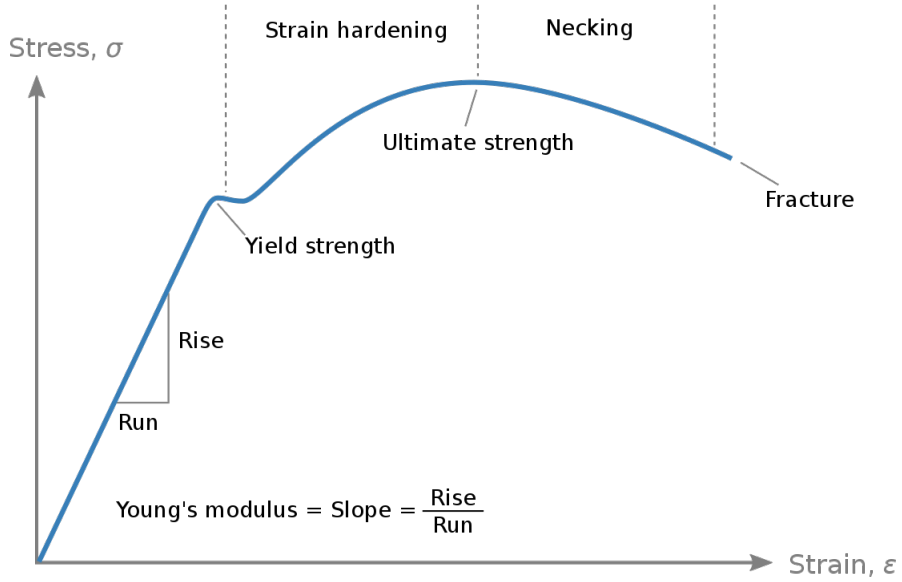

Figure 3.8: Stress as a function of the strain. Typical graph for an elastic material.

In the elastic domain the Young's modulus represents a constant of the material, differently from the plastic region. In the elastic region, the material recovers its initial shape when the applied forces are removed from the system. In the plastic region, the deformation of the material is permanent. The Young's modulus is a measurement of how hard is to deform a solid material in the tensile test. For example, for polymers (easy to deform) we have Young's modulus typically ranging from 0.1 to 10 GPa, while metals present a Young's modulus in the interval between 10 GPa and 200 GPa.[42]

3.2.3 Ferromagnetism

A very important concept used to describe the magnetic properties of ferromagnetic systems is the normalized magnetization, here symbolized by $\vec{m}$. The magnetization in a volume V of a material is defined as the sum of the magnetic moment $\vec{\mu}$ divided by the volume V. In its turn, the magnetic moment of a plane circular corrent I is $\vec{\mu} = I\vec{A}$, where the modulus of the vector $\vec{A}$ is the area of the circle, and its direction perpendicular to the current with orientation given by the right-hand rule. Figure 3.9 gives an illustration of the circular loop of current and the magnetic moment related to it.

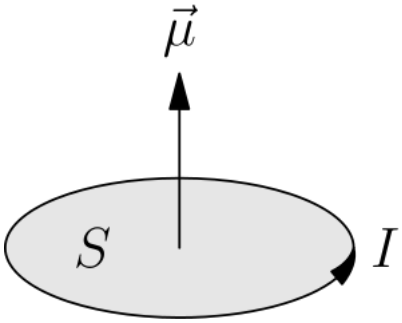

Figure 3.9: Illustration of a magnetic moment $\vec{\mu}$ generated by an electric current I in a disk

Every material can be classified in states of matter. A common and beginner-level example is the classification of physical state of matter as solid, liquid, and gas, just to name a few (there are more states inside this classification, as elastomer and Bose-Einstein condensate). It is a common practice, even in scientific enviroments, to give the material an informal and rigorous-lacking way label (liquid, for instance), forgetting the important aspect that this is not a permanent aspect of matter, but a state that depends on external parameters, such as temperature and pressure.

The most important classification considered in this work is the magnetic states of matter, that can be: diamagnetic, paramagnetic, ferromagnetic, ferrimagnetic, and antiferromagnetic[43]. It is worth noticing that such states present intersections between them. It is to say, a material can present a diamagnetic and a ferromagnetic behavior at the same time. Although the main focus of our work is on flexible ferromagnetic membranes, we present a brief discussion on paramagnetic, diamagnetic, and ferromagnetic states of matter. A paramagnetic system consists of a state in which the magnetic moments of the atoms or molecules of the material are randomly orientated. While diamagnetic systems consists of a state regarding the induced change in the orbital motion of electrons due to an applied magnetic field. On the other hand, another way to characterize paramagnetic and diamagnetic systems are by the sign of their magnetic susceptibility χ: positive, for paramagnetic systems, and negative for diamagnetic ones. In many materials, we have a directly relation between the external applied field $\vec{H}$ and the magnetization $\vec{M}$, given by the following equation:

$$\vec{M} = \chi \vec{H} \tag{3.8}$$

Paramagnetic and diamagnetic systems obey eq. (3.8). But, there are other materials in which χ does not satisfy eq. (3.8). For instance, in ferromagnetic systems, the graphic describing the magnetization as a function of the magnetic field is not a well-deffined function because the magnetization depends on the history of the applied field. Fig. 3.10 illustrates the phenomenon of magnetic hysteresis, in which, the magnetization increases as a function of the magnetic field until it reaches the so-called saturation magnetization M_s when the material is under the action of an increasing magnetic field $\vec{H}$. After reaching the point of maximum magnetization, if we decrease the external field, the magnetization decrease in a different curve (the upper curve, from point “a" to point “b" in Fig. 3.10). In this context, when the magnetic field vanishes, the magnetization does not disappear. Actually it assumes a non-zero value, called remanence magnetization M_r. To reverse the magnetization direction, we need

to apply a magnetic field in the opposite direction, which produces a decrease in the magnetization, until it vanishes, under the action of the coercive magnetic field H_c.

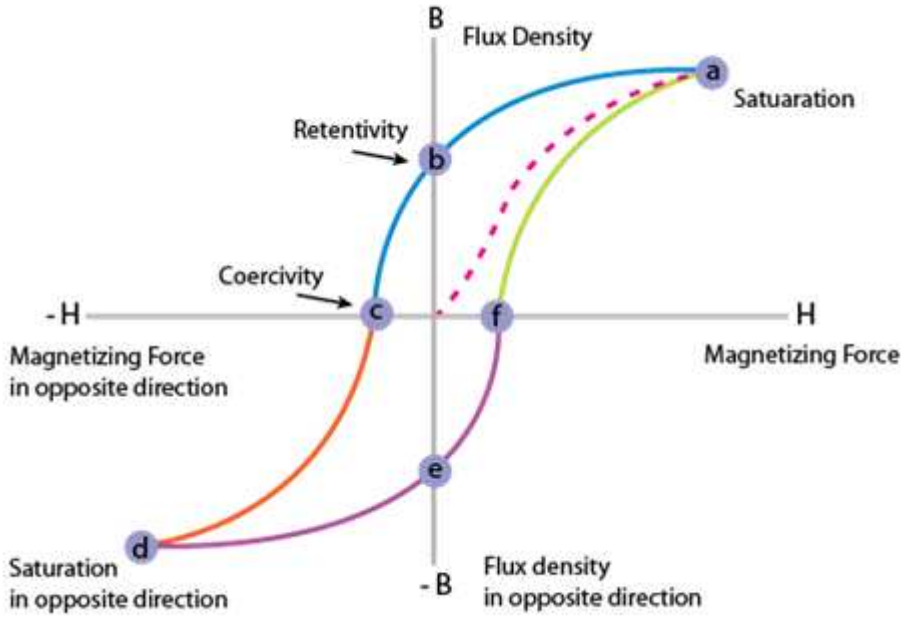

Figure 3.10: Hysteresis cycle of a ferromagnetic material. The magnetization M is put as a "function" of the external field H and its physical history.

3.2.4 Merons

Due to the competition between different magnetic interactions, possible magnetic states that appear in nanodisks are vortices and antivortices. In the context of field theory, these quasi-particle states are called merons, and can be classified as topological objects having topological charge $Q = 1/2$ (vortices) and $Q = -1/2$ (antivortices) [3]. Therefore, in this work, we refer vortices and antivortices as merons. To represent the meron's profile, we use the following ansatz:

$$\begin{cases} \Theta(\rho) = \arccos\left(\dfrac{p}{1+(\frac{\rho}{r_0})^s}\right) \\ \Phi(\phi) = (q-1)\phi + \gamma \end{cases} \tag{3.9}$$

where p, q, and γ are respectively the polarity, winding number, and chirality of the meron. Additionally, r_0 and s determines the radius of the meron's core. The meron's polarity can assume the values $p = \pm 1$, where a negative polarity means an anti-parallel magnetization with respect to the normal in the core's region. A positive polarity means that the normal vector and the magnetization field points in the same direction. The winding number q accounts to determine the type of meron we are considering. That is, for $q = 1$ we have a vortex, while $q = -1$ describes an antivortex configuration. Finally, γ accounts to the angle between the magnetization and the radial direction. The parameters ρ and ϕ are the curvilinear coordinates that correlates with the Cartesian coordinates $x = \rho\cos\phi$ and $y = \rho\sin\phi$. The functions

[3] The images of vortices and anti-vortices can be see in 3.11

$\Theta(\rho,\phi)$ and $\Phi(\rho,\phi)$ determine the configuration of the magnetic field, given by the normalized magnetization $\vec{m} = \vec{N}/||\vec{N}||$ as a function of the geometric parameters θ and ϕ:

$$\vec{N} = \cos\Phi \sin\Theta \hat{n}_\rho + \sin\Phi \sin\theta \hat{n}_\phi + \cos\theta \hat{n} \tag{3.10}$$

The normalized vectors $\hat{n}_\phi$, $\hat{n}_\rho$ and $\hat{n}$ appearing on the magnetization are given by:

$$\begin{cases} \hat{n}_\phi = \dfrac{\partial_\phi \vec{r}}{|\partial_\phi \vec{r}|} \\ \hat{n}_\rho = \dfrac{\partial_\rho \vec{r}}{|\partial_\rho \vec{r}|} \\ \hat{n} = \dfrac{n_\phi \times n_\rho}{|n_\phi \times n_\rho|} \end{cases} \tag{3.11}$$

Images of the geometric/visual aspects of merons are presented in Fig. 3.11 for different values of winding number q, and the curvature parameter c. In a disk, a vortex preserves the symmetry under rotation around its main axis. I.e., if one rotates the disk around its symmetry-axes in an arbitrary angle, no differences among the magnetic micro-states are observed. Following the opposite behavior, AV would not preserve this symmetry.

q	-1	-1	-1	1	1	1
c	-1	0	1	-1	0	1
	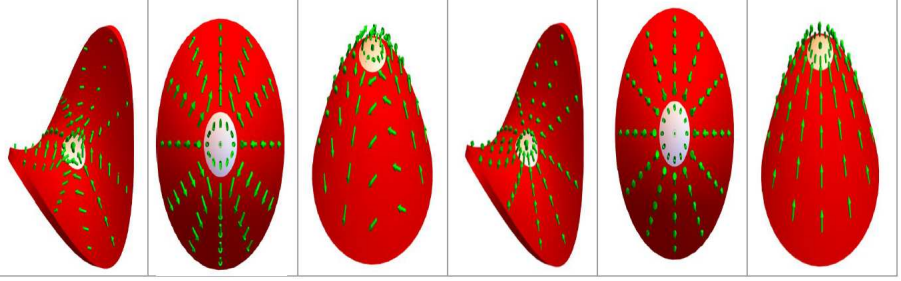					

Figure 3.11: Normalized magnetization field in the disk ($c = 0$), in the paraboloid ($c = 1$) and in the hyperbolic-paraboloid ($c = -1$) for some winding number values

Fig.3.12 shows the magnetic field of the meron's core, where we present a top view of a vortex with chirality $\gamma = \pi/2$ and winding number $q = 1$, lying on a paraboloidal surface. From the analysis of the central magnetic moment, it is clear that the polarity's sign determines whether the magnetization points up or down.

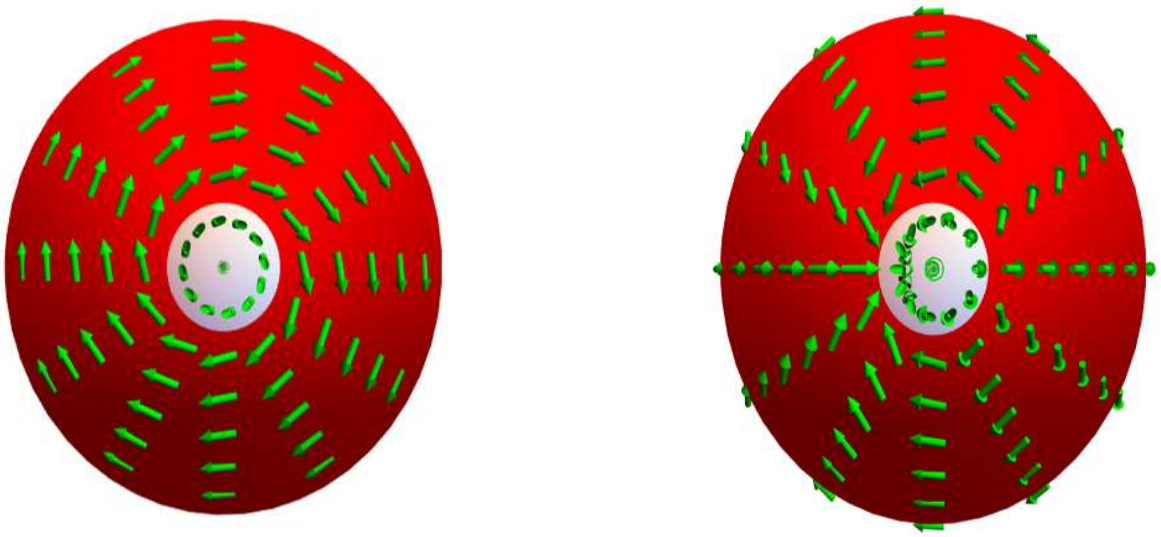

(a) $q = 1$ (b) $q = 2$

Figure 3.13: A vortex with winding number q in a ferromagnetic surface.

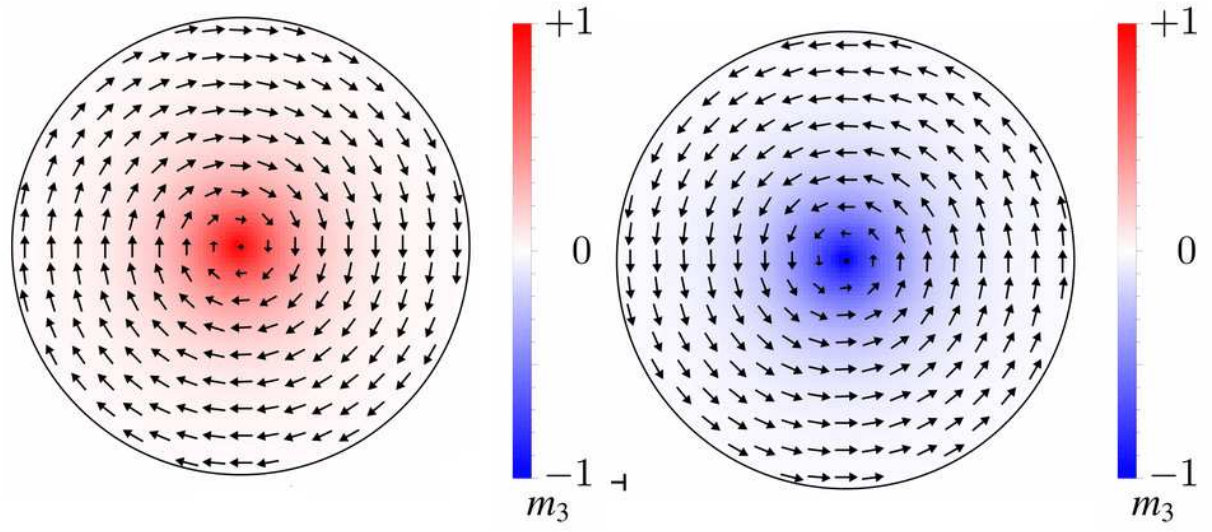

(a) Positive polarity $p = 1$ (b) Negative polarity $p = -1$

Figure 3.12: Fig. extracted from (44). Disks hosting a vortex configuration with (a) positive polarity (in red) (b) negative polarity (in blue).

The chirality γ gives an angle in the interval $[0, \pi]$, between the magnetization and the radial direction of the surface. For example, for $\gamma = \pi/2$ we have a circular magnetic field, depicted for the shape of a disk in Fig. 3.13-a.

The winding number is contained in the integer's set $\mathbb{Z} = \{..., -2, -1, 0, 1, 2, ...\}$. Its modulus $|q|$ encapsulates an important information, if $|q| = N$ the magnetization turns N times around the radius vector of the surface. Figs. 3.13 a and b depict a vortex configuration for $q = 1$ and $q = 2$, respectively.

3.3 Magnetic Energy

In this work, we consider that the magnetic energy of the ferromagnetic quasi-2D system is composed by an easy-surface effective anisotropy E_{ani} and the exchange energy E_{ex}. Additionally, we also consider the Zeeman interaction, which appears in situations where the quasi-2D system is under the action of an external magnetic field.

3.3.1 Anisotropy and Exchange energies

The expression for the anisotropy energy is defined bellow:

$$E_{ani} = K_a h \int (\vec{m} \cdot \vec{n})^2 \sqrt{g} \rho \theta \tag{3.12}$$

where the integration is performed along all the considered surface. The anisotropy energy vanishes when the normalized magnetization vector $\vec{m}$ is perpendicular to the vector $\vec{n}$, normal to the surface. On the other hand, $(\vec{m} \cdot \vec{n})^2$ assumes its maximum value when $\vec{m}$ and $\vec{n}$ have parallel directions. Because K_a is a positive constant, we have that the configuration that minimizes the energy is such that the normalized magnetization and the normal vector are perpendicular to each other. As a consequence of this fact, the anisotropy term forces the magnetization to be tangential to the surface. Fig. 3.14 shows two extreme situations.While Fig. 3.14-a depicts the vector configuration in which the anisotropy reaches its minimum value, 3.14-b shows the opposite case, where the anisotropy energy is maximum.

Since the anisotropy favours magnetization to be tangent to the surface, its presence contributes to diminish and control the size of the meron's core. Otherwise, the size of the meron's core would be the same as the disk's size once the exchange energy is minimized in this situation. Indeed, in the case of ferromagnetic systems, the exchange energy forces the spin of the neighbor magnetic ions in the lattice site to align parallel to each other.

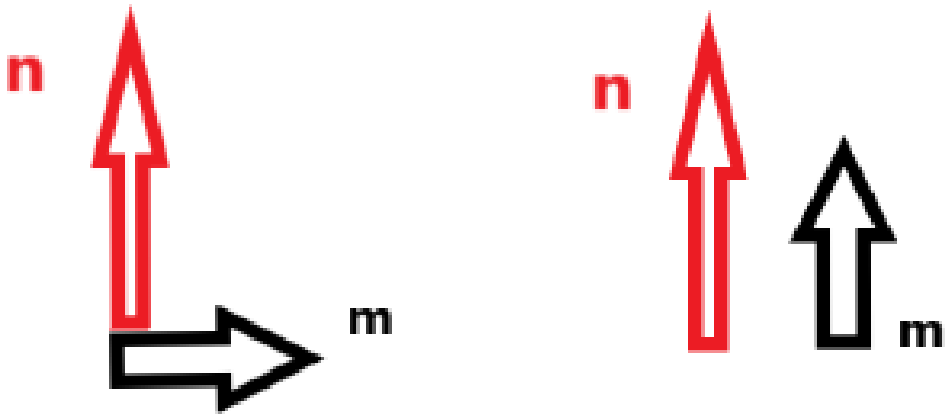

(a) Low anisotropy energy. (b) High anisotropy energy.

Figure 3.14: Two extreme situations between the normal vector $\vec{n}$ and the magnetization $\vec{m}$.

In a continuous approach, the expression to the exchange energy in a curved background is given by:

$$E_{exc} = Ah \int g^{\mu\nu} \frac{\partial \vec{m}}{\partial \mu} \cdot \frac{\partial \vec{m}}{\partial \nu} \sqrt{g} \rho \phi \tag{3.13}$$

where we utilized the Einstein notation, where repeated indices represents a sum. We have that $\mu, \nu = \rho, \phi$ and the elements $g^{\mu\nu}$ came from eq. (3.3) and eq. (3.2).

From the parameters A and K_a we can define the magnetic length as $\ell = \sqrt{A/K_a}$. We have used the parameters of Permalloy from Bryan *et al.*[45], therefore the exchange stiffness is given by $A = 10^{-11} J/m$, the saturation magnetization $M_s = 8.00 \times 10^3 A/m$, and the anisotropy constant is given by $K_a = \mu_0 M_s^2/2$, which is an effective anisotropy given by an approximation of the dipolar energy for small values of thickness[34].

3.3.2 Zeeman Energy

Finally, we also analyze the situation in which the considered system is under the action of an external magnetic field. In this case, there is the appearance of an extra term to the magnetic energy, so called Zeeman interaction. The Zeeman energy in a given volume of a certain material under the magnetic field B is given by an integration over its volume of the term $-\vec{M} \cdot \vec{B}$. As a proof of this statement, let represent the Lorentz force by $F = q_e(\vec{E} + \vec{v} \times \vec{B})$. In this context, the resulting work in the particle with charge q_e is:

$$E_Z = \int \vec{l} \cdot \vec{F}$$

Because the magnetic force is perpendicular to the velocity of the charged particles, there is no work produced during the particles motion. Therefore, we can simplify our analysis for considering that the Lorentz force can be reduced to the electric force $F_e = \int \vec{E} q_e = \int I \vec{E} t$. Then, we have:

$$E_Z = \int \vec{l} \cdot \left(\int tI\vec{E} \right)$$

By exchanging the order of the integrals, and moving the current term out of the inner integral (which is a constant over the lenght integral):

$$E_Z = \int tI \left(\int \vec{l} \cdot \vec{E} \right)$$

From the Maxwell's equations, one can use the Faraday's law in its integral form. Therefore, we can substitute the integral over the closed path $\int \vec{l} \cdot \vec{E}$ by the integral over the area encompassing the current $-\frac{}{t}(\int \vec{B} \cdot \vec{a})$. Therefore, we obtain:

$$E_Z = -I \int t \left(\frac{}{t} \int \vec{B} \cdot \vec{a} \right)$$

Thus, by using the Calculus Fundamental Theorem, the above equation can be simplified to

$$E_Z = -I \int \vec{B} \cdot \vec{a}$$

Finally, by using the fact that $I\vec{a} = \frac{1}{V} \int \tau I\vec{a}$, we have that

$$E_Z = -\int \vec{B} \cdot \left(\frac{I\vec{a}}{V} \right) \tau \tag{3.14}$$

One can see that the term inside the parenthesis in eq. (3.14) is the definition of the magnetization, and therefore we have finally arrived in the wanted equation of the Zeeman energy over a volume of a material:

$$E_{dip} = -\int \vec{B} \cdot \vec{m}\tau \tag{3.15}$$

3.4 Elastic Energy

The theoretical approach to calculate the elastic energy is based on the work of Efrati *et al.* [35], where the authors have considered a very thin structure with elastic and mechanical parameters given by the Poisson's ratio ν and Young's modulus Y. We assume that the initial shape of the quasi-2D system is a planar disk of radius R. Following the Efrati's ideas, we can consider that for small enough deformation of the disk we can state that the elastic energy is decoupled in two terms: the stretching energy, a term which acts against changes in the default area A_0 (i.e., the area of the planar nanodisk); and the bending energy, which tends to push the system to a planar state. Under these assumptions, we have that:

$$E_{elast} = E_{str} + E_b \tag{3.16}$$

where, the stretching energy E_{str} and bending energy E_b measures how much the surface deforms (in area and in shape). These elastic energy terms are given by an integration along the surface's area of the quasi-2D system. Efrati *et al.*[35] have obtained that stretching energy has a power of the thickness h, while the bending energy is a multiple of the third power of the thickness. Therefore, if we define the reference metric as the disk surface, and denote it as $\bar{g}^{ij}$, we have that:

$$\begin{cases} E_{str} = h \displaystyle\int_0^{2\pi} \int_0^R w_s \sqrt{|\bar{g}|}\rho\phi \\ E_b = h^3 \displaystyle\int_0^{2\pi} \int_0^R w_b \sqrt{|\bar{g}|}\rho\phi \end{cases} \tag{3.17}$$

where, the stretching and bending energy densities are given by:

$$\begin{cases} w_s = \dfrac{Y}{8(1+\nu)} \left(\dfrac{\nu}{1-\nu} \bar{g}^{\alpha\beta}\bar{g}^{\gamma\delta} + \bar{g}^{\alpha\gamma}\bar{g}^{\beta\delta} \right) (g_{\alpha\beta} - \bar{g}_{\alpha\beta}) \left(g_{\gamma\delta} - \bar{g}_{\gamma\delta} \right) \\ w_b = \dfrac{Y}{24(1+\nu)} \left(\dfrac{\nu}{1-\nu} \bar{g}^{\alpha\beta}\bar{g}^{\gamma\delta} + \bar{g}^{\alpha\gamma}\bar{g}^{\beta\delta} \right) b_{\alpha\beta} b_{\gamma\delta} \end{cases} \tag{3.18}$$

where, the factor $b_{\alpha\beta} = \hat{n} \cdot \partial_\beta \vec{g}_\alpha$ is the second fundamental form. Eq. (3.18) evidences that the stretching the stretching and bending energy densities determine how distant

the quasi-2D system is from the reference metric. It is worth noticing that the factor $(g_{\gamma\delta} - \bar{g}_{\gamma\delta})$, means that the elastic energy increases when the surface differs from the planar disk (which is the free elastic-energy configuration).

Chapter 4

Results and Discussion

> "The study of physics is also an adventure. You will find it challenging, sometimes frustrating, occasionally painful, and often richly rewarding."
>
> Hugh D. Young

In this chapter, we present the results obtained from the presented theoretical model and the discussions. This part of the text is divided into three sections. Section "Curvature-Vorticity Conjecture" (sec. 4.1) presents the analysis of the magnetic energy of merons on different curved surfaces. The obtained results give evidences to state a conjecture that relates the curvature of the surface and the meron's winding number. The second section "Analytical Calculations" (sec. 4.2) consists of analytical calculations of the exchange energy of a vortex configuration lying on a disk and on paraboloidal surface, confirming previously obtained results[46]. Finally, section "Magnetoelastic quasi-2D system" (sec. 4.3) presents the analysis of the properties of flexible magnetic disks as a function of mechanical and magnetic parameters, such as the external radius of the nanodisk, the Young's modulus, and the meron's chirality. We also present the analysis of the behavior of the flexible magnetic nanodisk under the action of an external magnetic field $\vec{B} = -B\hat{z}$.

4.1 Curvature-Vorticity Conjecture

To give more robustness to the conjecture that establishes a relationship between the winding number of the meron (vortex or anti-vortex) and the surface's curvature sign, in this subsection, we present in addition to the main parametrization P1, two other parametrizations to describe a flexible magnetic structure hosting a meron as a metastable state. First, we state the conjecture and after that we give the parametrizations, their Gaussian curvatures, and the energy of the system as a function of the curvature parameter c.

Conjecture (Curvature-Vorticity Conjecture). If a magnetic system is described just by the exchange energy, where the chirality γ and the polarity p are such that the energy is minimized; and the core' radius is at least an order of magnitude smaller

then the surface's radius $r_0 < 0.3R$, then the position of the Gaussian curvature $K = 0$ (with an error smaller then 5%) gives $E_V = E_{AV}$. Also, if $K > 0$ the vortex has smaller exchange energy then the anti-vortex. If $K < 0$, the opposite occurs.

4.1.1 Main Parametrization P1

The main parametrization considered in this work consists of a confirmation of the results obtained by Elías *et al.*[4]. The description made by the authors was of rigid surfaces in which its energy was given by the exchange and anisotropy energy. In this case, the geometrical description of the surface is given by:

$$\vec{r} = (x, y, c(cx^2 + |c|y^2)) \tag{4.1}$$

where $c \in [-1, 1]$ is a parameter of curvature that satisfies the sign relation with the Gaussian curvature $K(x, y)_{\pm} = c_{\pm}$. In Fig. 4.1 we show the behavior of the magnetic energy as a function of c for merons with different winding numbers. Red squares depicts the energy of the vortex state, while black circles regards the energy of the antivortex configuration.

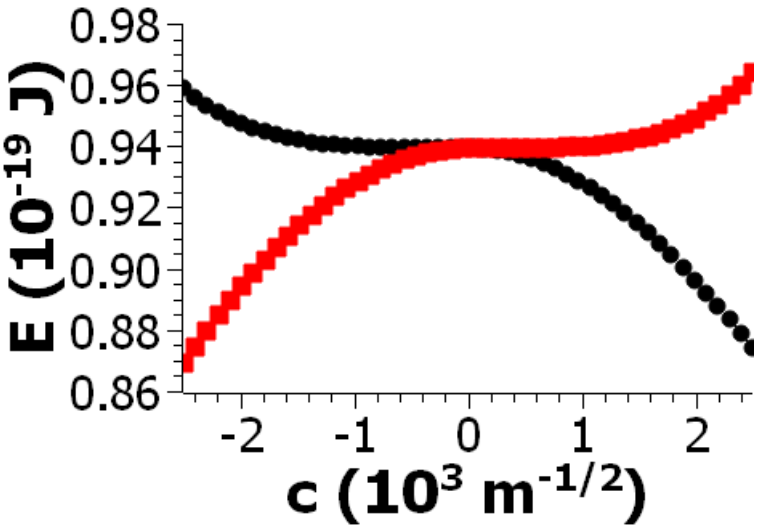

Figure 4.1: Magnetic energy as a function of the curvature parameter. The surface hosting vortex are depicted in red squares and the ones hosting anti-vortex are depicted in black circles.

Analyzing Fig. 4.1, we conclude that negative Gaussian curvature surfaces hosting anti-vortices have lower energy than those ones with positive Gaussian curvature. On the other hand, for surfaces hosting vortices the preferred geometry (i.e., the geometry giving the lower energy) are the ones with positive Gaussian curvature. In Fig. 4.2, we present two of the considered geometries and their respective minimum energy merons. That is, the paraboloid hosting a vortex (a) and the hyperbolic paraboloid hosting an anti-vortex (b).

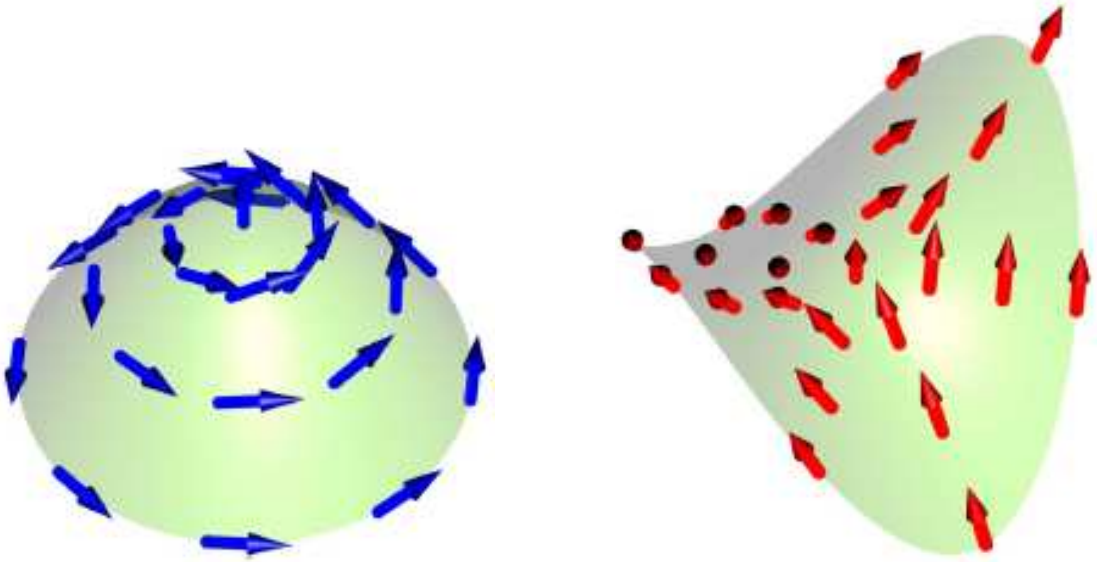

(a) a paraboloid hosting a vortex-configuration

(b) a hyperbolic paraboloid hosting an anti-vortex configuration

Figure 4.2: Figure extracted from Elias *et al.*[4].

From this example, we conclude that the inequality $q \cdot K > 0$ holds. Therefore, positive Gaussian curvature ($K > 0$) surfaces hosts vortex ($q > 0$), while negative ones ($K < 0$) hosts anti-vortex ($q < 0$). Figure 4.1 shows in red squares the graph of the magnetic energy as a function of the curvature c when the magnetization configuration is of vortex and in black squares the same graph for an anti-vortex configuration. We can conclude that for the hyperbolic paraboloid (surface of negative Gaussian curvature), the anti-vortex configuration has a smaller energy than the vortex configuration. When the surface has the shape of a disk ($c = 0$), both magnetic configurations (vortex and anti-vortex) have the same energy. And finally, when the surface is a paraboloid (positive Gaussian curvature) the vortex is the configuration of minimum energy, when compared to the anti-vortex state.

4.1.2 Parametrization P2

The second considered parametrization is given by:

$$\vec{r} = (x, y, d(x^2 + y^2) + cxy) \tag{4.2}$$

where, we define two constants with relation to the variables x, y. The constant $d = 1$ m^{-1} and the curvature parameter c with the same dimension of d. These constants are introduced in order to give consistence for the unity of the vector that defines the surface shown in eq. (4.2). When the curvature parameter is $c = 3$, the surface is given by the hyperbolic paraboloid shown in 4.3-c. If $c = \pm 2$, the surface is a parabolic cylinder (See Fig. 4.3)-b. And finally, when $c = 0$, we have the shape of a sphere (see Fig. 4.3-a).

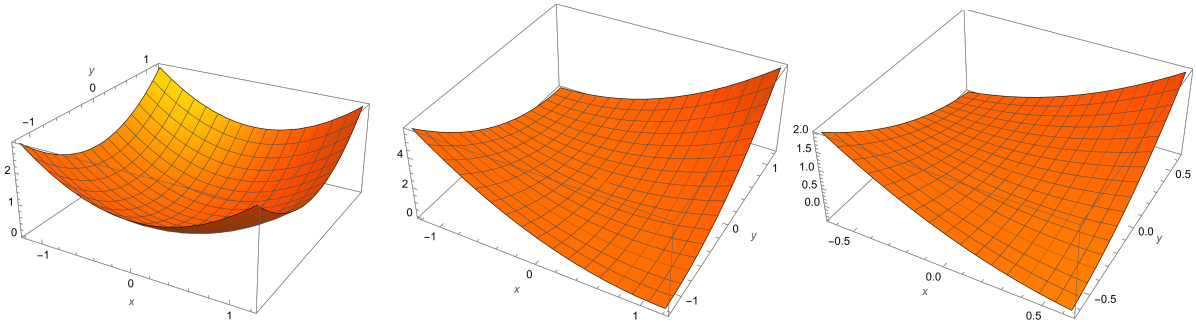

(a) $c = 0$ (b) $c = 2$ (c) $c = +3$

Figure 4.3: Examples of surfaces from parametrization 4.2. From left to right: a) Positive Gaussian Curvature, b) Zero curvature, c) Negative Curvature.

Using the surface function $F(x, y) = d(x^2 + y^2) + cxy$ and the definition of the Gaussian curvature 3.4, one is able to compute the Gaussian curvature as a function of the Cartesian coordinates and the constant c, as follows:

$$K(x, y) = \frac{4d^2 - c^2}{(1 + (2dx + cy)^2 + (2dy + cx)^2)^2} \tag{4.3}$$

Therefore, the sign of the Gaussian curvature is determined by the parameter c, and can be expressed by:

$$K_{\pm} = \begin{cases} 1 & \text{, if } |c| < 2 \\ 0 & \text{, if } |c| = 2 \\ -1 & \text{, if } |c| > 2 \end{cases} \tag{4.4}$$

We have used the notation $K_{\pm}$ to denote the sign of the Gaussian curvature for the parametrization T2. The sign function $K_{\pm}$ is: 1 if $K(x, y) > 0$, 0 if $K(x, y) = 0$, and -1 if $K(x, y) < 0$.

From the Curvature-Vorticity conjecture, we would expected that for $c < -2$ and $c > 2$, the AV configuration would yield to a smaller energy if we compare it with the V configuration. For $-2 < c < 2$ the V configuration would be the stable state. Finally for $c = \pm 2$, both configurations should have the same exchange energy.

From comparing the predictions followed by the conjecture with the graph 4.4, we promptly notice that they agree with each other. Indeed, although the value of c for which the curves describing the energy of V (black circles) and AV (red squares) configurations intersect are not exactly $c = -2$ and $c = 2$, they are in a region containing these points with a error-radius of less the 5%. This error could be a influence of the mean curvature of the surface, which is also important to determine the magnetic properties of curved structures.[26]

4.1.3 Parametrization P3

Finally, the third parametrization we have considered is given by

$$\vec{r} = \left(x, y, \frac{x^6}{30} + c(1 - c)y^2\right) \tag{4.5}$$

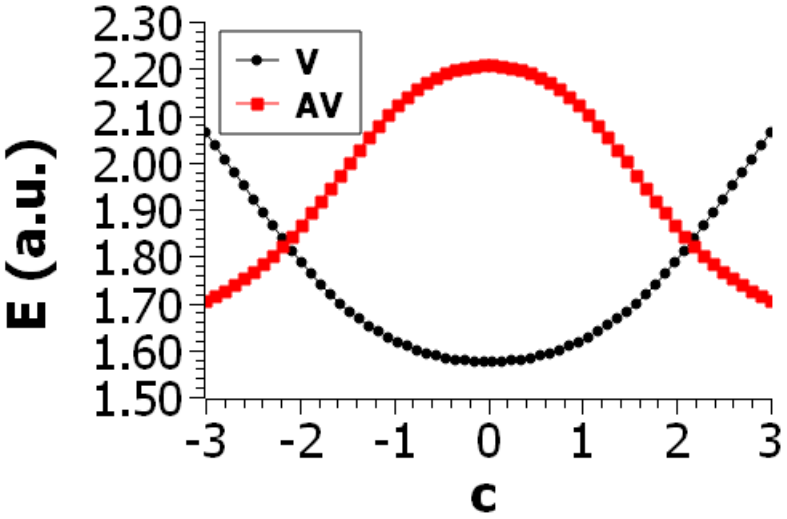

Figure 4.4: Exchange energy as a function of c.

One can notice that we have omitted constants (multiplying $\frac{x^6}{30}$ and cy^2) to give $F(x,y) = \frac{x^6}{30} + c(1-c)y^2$ the dimension of meters. Instead, we assume these dimensional parameters being equal to one. It is to say, if one gives to x and y the value of meters, the Gaussian curvature is then given by m^{-2}. The equation of the Gaussian curvature coming from eq. (4.5) is cumbersome, and we do not present it in this work. Nevertheless, we are interested in analyzing the relationship between the meron's winding number and the Gaussian curvature sign of the quasi-2D system. Therefore, we present the sign of the Gaussian curvature as a function of c, which behaves as follows:

$$K_{\pm} = \begin{cases} 1 & \text{, if } 0 < c < 1 \\ 0 & \text{, if } c = 0 \text{ or } c = 1 \\ -1 & \text{, if } c < 0 \text{ or } c > 1 \end{cases} \tag{4.6}$$

Fig. 4.5 presents the shape of structures described by the parametrization given in eq. (4.5). Figures a, b, and c depict respectively, the shapes for a surface with positive, zero, and negative Gaussian curvature.

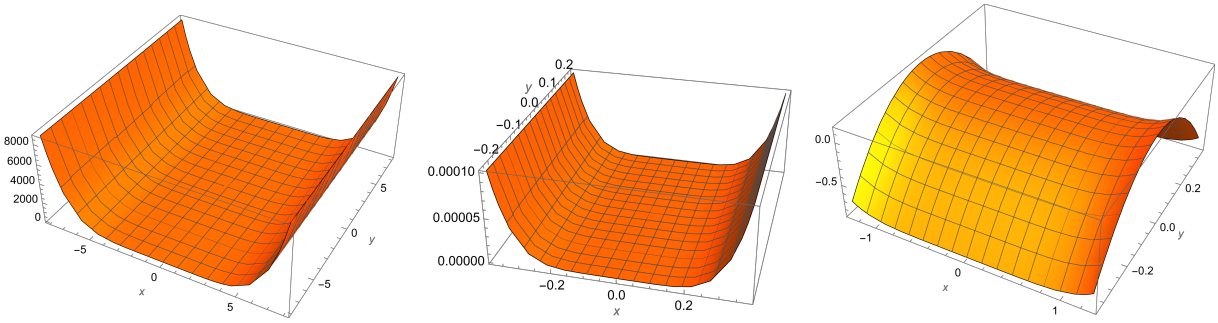

(a) $c = 0.5$ (b) $c = 1$ (c) $c = +3$

Figure 4.5: Examples of surfaces from parametrization P3. For (a) Positive , (b) zero , and (c) negative Gaussian curvature

Again, we notice an agreement between the Curvature-Vorticity Conjecture and

the theoretical result illustrated by Fig.4.6. Indeed, one can see that while the AV state minimizes the energy (when compared with the V state) for $c < 0$ and $c > 1$, the V state is the metastable state for $0 < c < 1$. Because the Gaussian curvature is almost the same for $c = 0.5$ and $c = 1$, we have a very narrow difference between the graphs for V and for AV on these points.

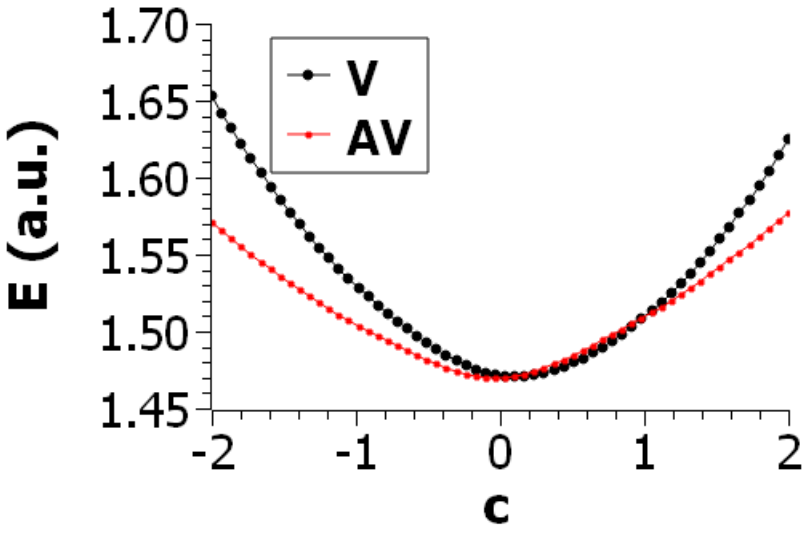

Figure 4.6: Transformation T3: Graphic of the exchange energy in function of the curvature parameter c.

Since three different transformations point to the same relationship between the Gaussian curvature and the meron's winding number, we can conjecture, by induction, that the Curvature-Vorticity connection is true for every transformation. The formal proof for this conjecture is an interesting issue, and will be subject of future investigations.

4.2 Exchange energy of the vortex configuration in planar and paraboloidal structures

In order to obtain analytical results and compare them with previously obtained determining the energy of vortices when they are hosted in very thin nanodisks[34] and paraboloidal[46] structures. Here, we explicitly determine the analytical expression of the exchange energy in the region $r > r_0$. In this context, we restrict this analysis when the magnetic parameters of the vortex are given by $\gamma = 0$, $p = 0$ e $q = 1$. Therefore eq. (3.9) is simplified to:

$$\begin{cases} \Theta = \dfrac{\pi}{2} \\ \Phi = 0 \end{cases} \tag{4.7}$$

Thus the magnetization $\vec{N}$ and the normalized magnetization $\hat{m}$ are given by:

$$\begin{aligned}\vec{N} &= \cos\Phi \sin\Theta \hat{n}_\rho + \sin\Phi \sin\theta \hat{n}_\phi + \cos\theta \hat{n} \\ \vec{N} &= \hat{n}_\rho \\ \hat{m} &= \hat{n}_\rho\end{aligned} \tag{4.8}$$

4.2.1 Disk

The geometry of the disk can be obtained from taking $c = 0$ in Eq. (3.1). In this context, we have that:

$$\vec{r} = (\rho\cos\phi, \rho\phi, 0) \tag{4.9}$$

Once $\hat{n}_\nu = \frac{\vec{g}_\nu}{||\vec{g}_\nu||}$, where $g_\nu = \partial_\nu \vec{r}$ e $\nu = \rho, \phi$, we should have:

$$\begin{cases}\hat{n}_\rho = (\cos\phi, \phi, 0) \\ \hat{n}_\phi = (-\phi, \cos\phi, 0)\end{cases} \tag{4.10}$$

Therefore, the normalized magnetization can be explicitly written as $\hat{m} = (\cos\phi, \phi, 0)$. Then, calculating the components of the counter-variant metric tensor we get to the following result:

$$\begin{cases}g^{11} = \rho \\ g^{12} = g^{21} = 0 \\ g^{22} = \dfrac{1}{\rho^2}\end{cases} \tag{4.11}$$

Finally, the exchange energy can be calculated:

$$\begin{aligned}E_{exc} &= Ah \int_0^{2\pi}\int_{r_0}^{R} \left(g^{11}\frac{\partial\vec{m}}{\partial\rho}\cdot\frac{\partial\vec{m}}{\partial\rho} + 2g^{12}\frac{\partial\vec{m}}{\partial\rho}\cdot\frac{\partial\vec{m}}{\partial\phi} + g^{22}\frac{\partial\vec{m}}{\partial\phi}\cdot\frac{\partial\vec{m}}{\partial\phi}\right)\sqrt{g}\phi\rho \\ &= Ah\int_0^{2\pi}\int_{r_0}^{R}\frac{1}{\rho}\phi\rho \\ &= 2\pi Ah\ln\left(\frac{R}{r_0}\right)\end{aligned} \tag{4.12}$$

4.2.2 Paraboloid

For a paraboloidal surface, the parametrization is given by $\vec{r} = (\rho\cos\phi, \rho\phi, c^2\rho^2)$, yielding the following counter-invariant elements:

$$\begin{cases}g^{11} = \dfrac{1}{1+4c^4\rho^2} \\ g^{12} = g^{21} = 0 \\ g^{22} = \rho^{-2}\end{cases} \tag{4.13}$$

Therefore,

$$
\begin{aligned}
E_{exc} &= Ah \int_0^{2\pi} \int_{r_0}^{R} \left(g^{11} \frac{\partial \vec{m}}{\partial \rho} \cdot \frac{\partial \vec{m}}{\partial \rho} + 2g^{12} \frac{\partial \vec{m}}{\partial \rho} \cdot \frac{\partial \vec{m}}{\partial \phi} + g^{22} \frac{\partial \vec{m}}{\partial \phi} \cdot \frac{\partial \vec{m}}{\partial \phi} \right) \sqrt{g} \phi \rho \\
&= 2\pi Ah \ln \left(\frac{R + \sqrt{1 + 4c^2 r_0^2}}{r_0 (1 + \sqrt{1 + 4c^2 R^2})} \right)
\end{aligned}
\tag{4.14}
$$

The exchange energy given Eq. (4.14) is in agreement with the results obtained in [46]. In the special case where the paraboloid is deformed to a disk ($c \to 0$) we recover the result given in Eq. (4.12), as should be.

4.3 Magnetoelastic quasi-2D system

In the work of Elías *et al.* [4], the authors did not take into account the elastic energy. Therefore, to diminish the magnetic energy, the system deforms indefinitely to reach the shape presenting the minimum energy configuration.

In this section we present the results concerning the relation between the magnetic and mechanical subsystems to determine the equilibrium shape of the nanostructure hosting a meron as metastable state. Therefore, we analyze a set of parameters of the quasi-2D system and its behavior in terms of optimum curvature and energy.

4.3.1 Radius

Firstly, we determine the influence of the external radius of the disk on the equilibrium shape. Therefore, we set the thickness as $h = 0.1\ell$ and the Young's modulus given by $A/(Yh^2) = 40$. We have then investigated the total energy of the structure as a function of c considering different values to the radius of the nanodisk. Main results are depicted in Fig. 4.7, where we present the numerical results for nanostructures with radius a) 4ℓ, b) 6ℓ, c) 8ℓ, and d) 10ℓ.

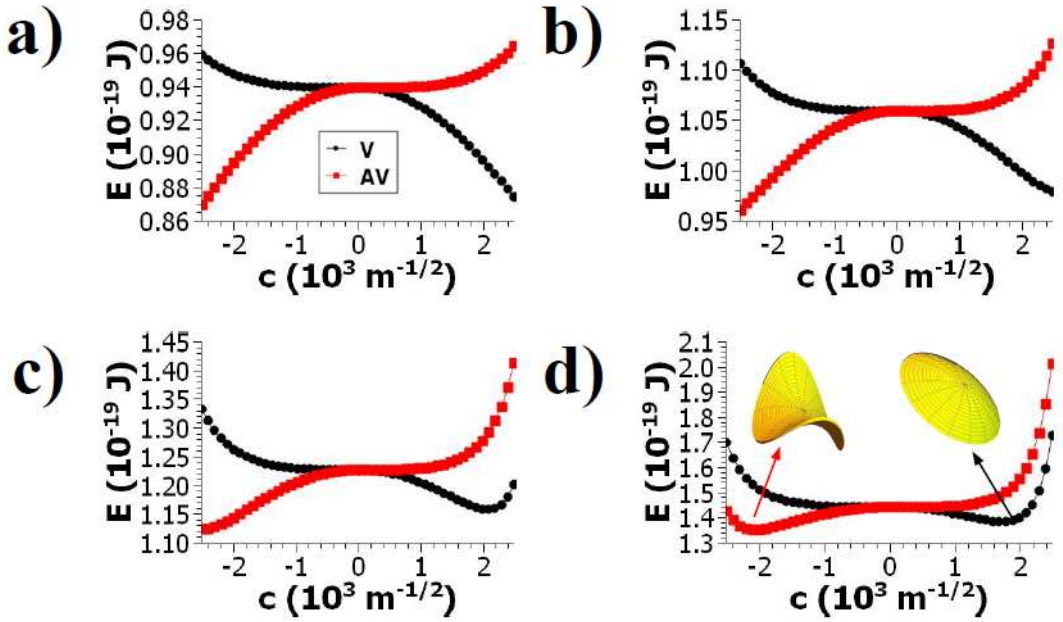

Figure 4.7: Total energy as a function of c for different disk radius. Figures a, b, c, and d present the results for $R = 4\ell$, 6ℓ, 8ℓ, and 10ℓ, respectively. The thickness is $h = 0.1\ell$, and $A/(Yh^2) = 40$.

We observe that for nanodisks with small radius (see Fig. 4.7-a) the flexible magnetic structure presents the same qualitative behavior obtained for rigid structures (see Fig. 4.1). Therefore, one can conclude that the elastic energy is negligible in comparison with the magnetic energy. Nevertheless, the analysis of Fig. 4.7 also reveals that the increase in the radius of the nanostructure yield an increase in the elastic contribution to the total energy.

Fig. 4.7 shows that an increase in radius, makes the equilibrium value c^* near the origin. For example, for radius $R = 4\ell$ (See Fig. 4.7-a) the equilibrium curvature for vortex and anti-vortex is in their extremes, while for $R = 10\ell$ (See Fig. 4.7-d) the equilibrium value is $c = -2.1 \times 10^3\ m^{-1/2}$ for the vortex, and $c = +1.8 \times 10^3\ m^{-1/2}$ for the anti-vortex. We conclude that it is more difficult to bend and stretch the quasi-2D system for large values of radius. Therefore, there is a critical value of c from which the increase in the elastic energy avoids the system continue to deform. Then, at this value, we obtain the optimum curvature for a flexible nanodisk hosting a meron as magnetization state. For instance, Fig. 4.7-d, shows that with external radius of $R = 10\ell$ the curvature parameter of a system hosting antivortex merons is $c = -2.1 \times 10^3\ m^{-1/2}$, while for the system hosting a vortex the optimum curvature parameter is $c = +1.8 \times 10^3\ m^{-1/2}$. It can be also noticed that in all presented cases, the Curvature-Vorticity conjecture is obeyed. That is, surfaces with positive curvature host vortices, while surfaces with negative curvature host antivortices as metastable states.

Elastic Energy

In this subsection we present the graphs of the stretching and bending energy for different values of the external radius of the quasi-2D system fixing the same values as in the last subsection. From the analysis of Fig. 4.8, we observe that the bending energy is three order of magnitude smaller than the stretching energy. This facts

comes from the fact that we are considering very thin systems. Thus, the bending energy is orders of magnitude smaller that the stretching because while the stretching energy is a multiple of h, the bending energy depends on h^3. Also, it is worth noticing that as the quasi-2D system deviates from its initial state (a planar disk), there is an energy cost to deform the nanostructure. Therefore, when the system deforms, the increase in the elastic energy is responsible for bring the system to its equilibrium shape. Finally, by comparing the results presented in Figs. 4.7-d and 4.8-d, it can be noticed that the elastic energy presents a pronounced increase when the system reaches its optimum curvature.

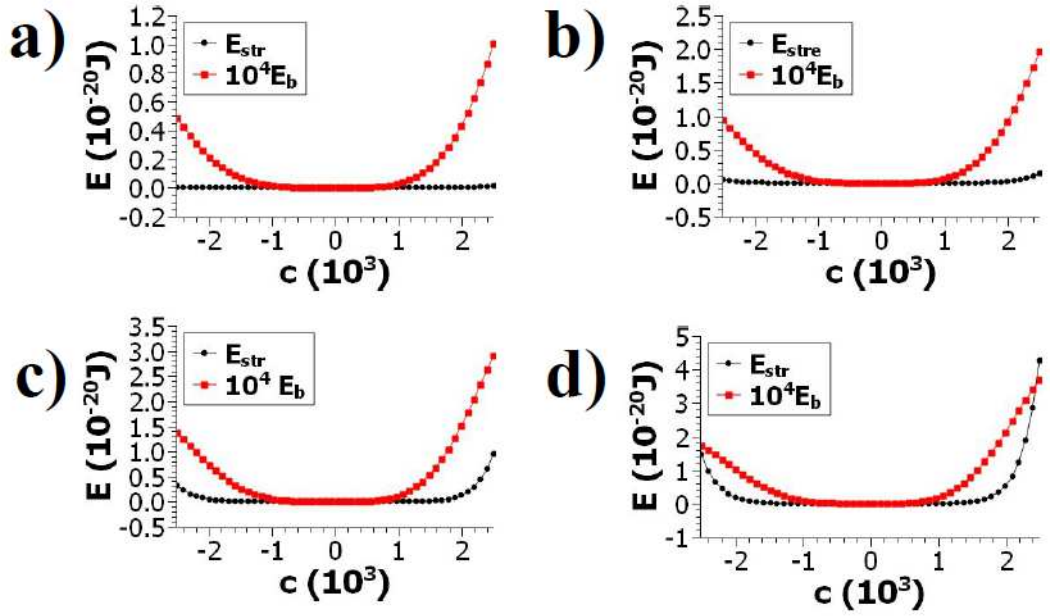

Figure 4.8: Stretching E_{str} and bending energy E_b as a function of c for different disk radius. Figures a, b, c, and d present the results for $R = 4\ell$, 6ℓ, 8ℓ, and 10ℓ, respectively. The thickness is $h = 0.1\ell$, and $A/(Yh^2) = 40$.

4.3.2 Young's modulus

After analysing the influence of the external radius on the optimum curvature, we study the dependence of the nanodisk shape on the Young's modulus value. In Fig. 4.9, we present the meron's energy as a function of c for the cases: $A/(Yh^2)$ a) 400, b) 40, c) 8, and d) 4. We highlight the fact that changes in the Young's modulus modify only the elastic term and the total energy. Therefore, to analyze the behavior of systems having different elastic properties, we have considered three main domains to the value of Y: a domain in which the elastic energy is much smaller than the magnetic energy (low value of Y), a domain in which elastic and magnetic energies terms compete, and a domain in which the elastic energy is big enough to make vortex and antivortex systems present the same total energy, independent of the shape of the nanostructure.

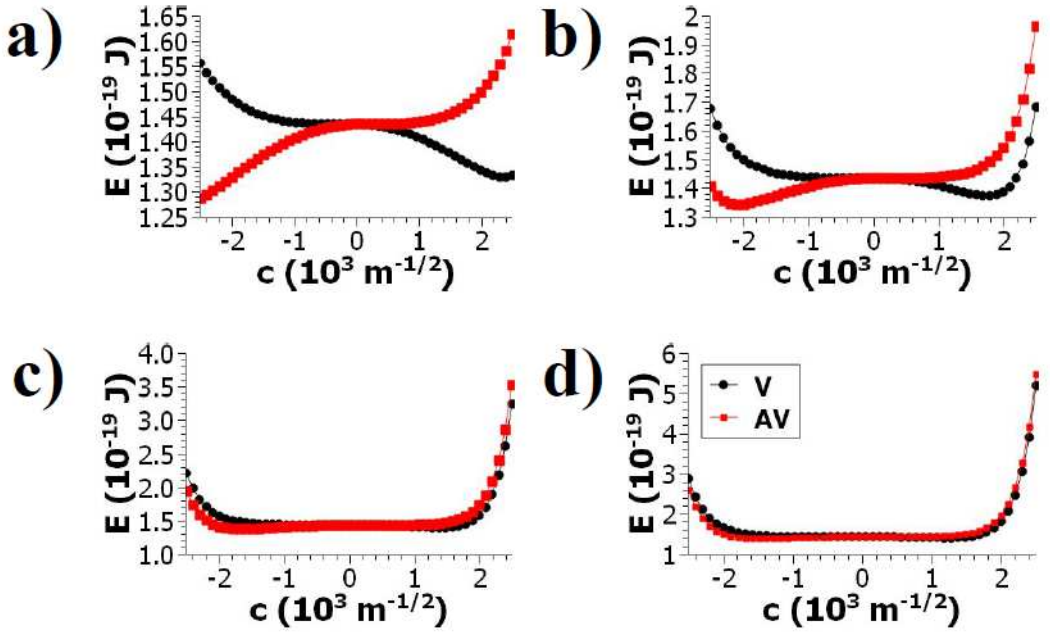

Figure 4.9: System energy as a function of the curvature for a nanodisk with radius $R = 10\ell$ and $h = 0.1\ell$ for different Young's modulus. Figures a, b, c, and d, depict a nanostructure with $A/(Yh^2) = 400$, 40, 8, and 4 respectively.

From the analysis of the results presented in Fig. 4.9, we conclude that the proper adjust of Y can be used for engineering shapeable systems. If Y is too high (Fig. 4.9d), it is very difficult to modify the shape of the quasi-2D system. On the other hand, if Y is too low (Fig. 4.9a), the quasi-2D system behaves as a surface without resistance to bending and stretching as the results became the same as the model which did not consider the elastic energy. For intermediate values of Y (Fig. 4.9b), the optimum value of the parameter c varies as we vary the material of the surface (and therefore its Young's modulus).

4.3.3 Chirality and Polarity

After analyzing the behavior of the system as a function of geometrical and mechanical parameters, we study the influence of the polarity and chirality of the meron on the curvature of the nanodisk. In this context, we consider a vortex with winding number q=1 and initial polarity p=1. Fig. 4.10 presents the optimum curvature c^* and its total energy E^* as a function of the chirality of the meron, when the polarity is fixed at $p = 1$ (Figures 4.10-a and b) and when the polarity is a step function assuming the value $p = 1$ for $\gamma \leq \pi/2$ and $p = -1$ for $\gamma > \pi/2$.

The obtained results evidence that it is possible to control the geometry of the quasi-2D system by controlling the vortex chirality γ. In Fig. 4.10-a we observe an increase in the chirality until the value of $\pi/2$ yields to a decrease in the positive curvature. In other words, one can control the curvature in the range $c \in [0, 1.5 \times 10^3 m^{-1/2}]$ by adjusting the chirality from zero to $\pi/2$. As the chirality surpass the limiting value of $\pi/2$ the system saturates to the state of a planar nanodisk with constant energy.

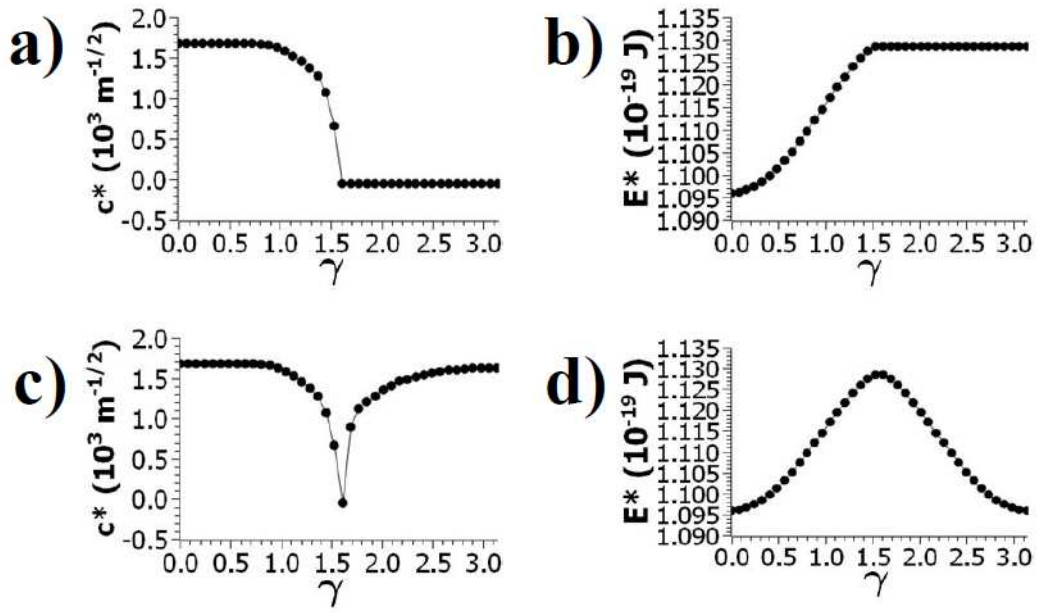

Figure 4.10: optimum curvature (a and c) and total energy (b and d) as a function of γ for a unchanged (top graphics) and variable (bottom graphics) polarity.

4.3.4 External Magnetic Field

To finish this section, we consider that the nanodisk is under the action of an external magnetic field pointing in the opposite direction of the initial vortex polarity. In this context, we have analyzed two different values to the magnetic field intensity, 0.5 mT and 5 mT. The Zeeman energy is a few orders smaller then the total energy (magnetic plus elastic energy). Therefore, the addition of an external field acts as a perturbation in the system. Nevertheless, even with the Zeeman interaction being small, even a magnetic field of 0.5 mT is enough to produce changes in the shape of the nanodisk. Additionally, from the comparison between the results for the magnetic fields of 0.5 mT and 5 mT, we observe that the increase in the value of the external magnetic field yields an icrease in the value of c that minimizes the total energy.

Also, the addition of the external magnetic field forces the appearance of a discontinuity of the energy of the optimum quasi-2D system as a function of the chirality, as one can see in Fig. 4.11 d). But this discontinuity is observed because we made the artificial transition of the polarity $p \leftarrow -p$, when chirality $\gamma > \pi/2$.

We conclude that it is possible to control a vortex in a quasi-2D system with a field of 0.5 mT. The control of the shape of the nanodisk by an external magnetic field can be done if we are able to modify not only its intensity but also its direction. With these two possibilities for controlling the geometry of flexible systems by an external magnetic field, one is able to change the shape of a nanomagnetic quasi-2D system and its position (which we have not explore in this work). Another important note is about the mechanical parameters of the quasi-2D system. We have used Young's modulus of $10^6\ N/m^2$, which is much smaller than a plethora of magnetic materials.

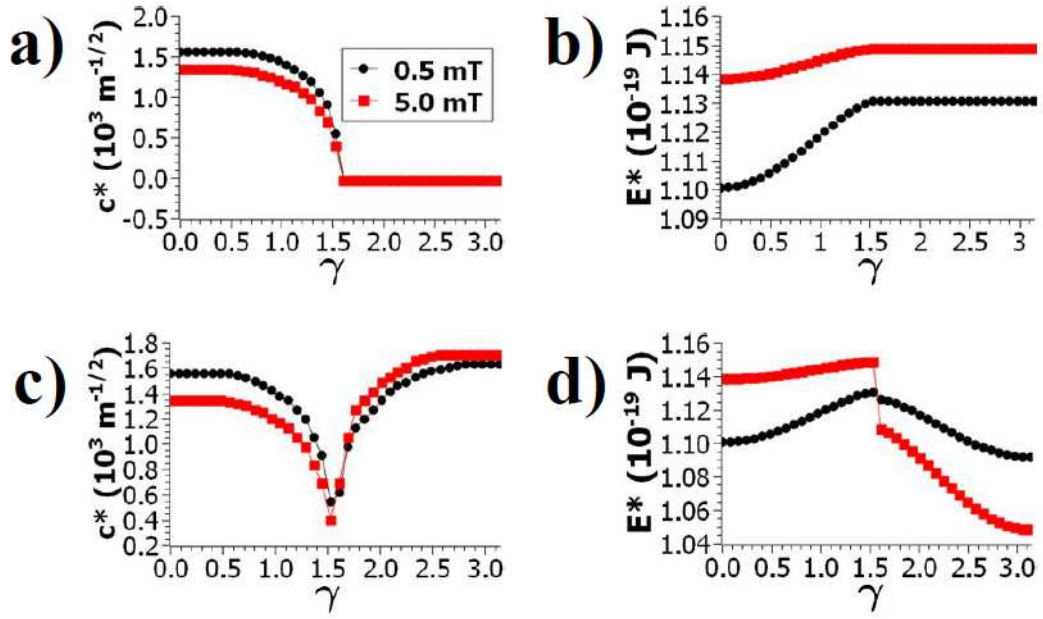

Figure 4.11: Optimum curvature and total energy for fixed (a and b) e variable (c and d) polarity as a function of the vortex chirality for a nanodisk under the action of a magnetic field $\mathbf{B} = -B\hat{\mathbf{z}}$. Black dots and red squares represent the results for $B = 0.5$ mT and $B = 5.0$ mT, respectively.

Chapter 5

Conclusion and Perspectives

> "One worthwhile task carried to a successful conclusion is better than fifty half-finished tasks."
>
> Bertie Charles Forbes

In this work we investigated the behavior of a nanodisk with small thickness and certain flexibility/elasticity. The nanodisk system had magnetic and mechanical energies and it was later on subject to an external magnetic field.

After an investigation to discover the origin of the relation between Gaussian Curvature sign and the meron's winding number's sign, we conclude that there is an intrinsic connection between these quantities due to curvature-induced exchange-driven effective interactions. We have then proposed a conjecture where the meron's winding number and the Gaussian curvatures sign depends one to each other. That is, surfaces with positive Gaussian curvature host vortices, while surfaces with negative Gaussian curvatures host antivortices as the lower energy metastable state.

We have demonstrated, through numerical results, that when the considered system hosts merons as magnetization configurations, the disk's radius, thickness, and the Young's modulus influence on the equilibrium shape of the flexible magnetic nanodisk. Increasing the radius, the thickness and the Young's modulus, generates a decrease in the value of the curvature that minimizes the energy. We also showed that there is a connection between the meron's polarity and chirality, which is also important in determining the equilibrium shape adopted by the considered flexible system.

It was also shown that a magnetic field can dictate the final shape of a ferromagnetic surface. For For instance, it was shown that a field of 0.5 mT is sufficient to control the nanodisk's geometry in a given range of curvature.

As a perspective for future works, we intend to perform Monte Carlo simulations to obtain new results and to confront them with the theoretical analytical results here presented.

Another action to further sustain the present work would be to verify, in a more formal mathematical demonstration, the result relating the relationship between the meron's type (V or AV) and the sign of the Gaussian curvature. This would give certainty to a more vast validity domain and would be useful in giving more information

and understanding the intrinsic connection between magnetic systems and curvature.

Bibliography

[1] M. Cianchetti, M. Calisti, L. Margheri, M. Kuba, and C. Laschi, "Bioinspired locomotion and grasping in water: the soft eight-arm octopus robot," *Bioinspiration & biomimetics*, vol. 10, no. 3, p. 035003, 2015.

[2] J. Bishop-Moser and S. Kota, "Towards snake-like soft robots: Design of fluidic fiber-reinforced elastomeric helical manipulators," in *2013 IEEE/RSJ International Conference on Intelligent Robots and Systems*, pp. 5021–5026, IEEE, 2013.

[3] Y. Cao, Y. Liu, Y. Chen, L. Zhu, Y. Yan, and X. Chen, "A novel slithering locomotion mechanism for a snake-like soft robot," *Journal of the Mechanics and Physics of Solids*, vol. 99, pp. 304–320, 2017.

[4] R. G. Elías, N. Vidal-Silva, and V. L. Carvalho-Santos, "Winding number selection on merons by gaussian curvature's sign," *Scientific Reports*, vol. 9, no. 1, pp. 1–7, 2019.

[5] M. Melzer, M. Kaltenbrunner, D. Makarov, D. Karnaushenko, D. Karnaushenko, T. Sekitani, T. Someya, and O. G. Schmidt, "Imperceptible magnetoelectronics," *Nature communications*, vol. 6, no. 1, pp. 1–8, 2015.

[6] H. Vandeparre, D. Watson, and S. Lacour, "Extremely robust and conformable capacitive pressure sensors based on flexible polyurethane foams and stretchable metallization," *Applied Physics Letters*, vol. 103, no. 20, p. 204103, 2013.

[7] R. C. Webb, A. P. Bonifas, A. Behnaz, Y. Zhang, K. J. Yu, H. Cheng, M. Shi, Z. Bian, Z. Liu, Y.-S. Kim, *et al.*, "Ultrathin conformal devices for precise and continuous thermal characterization of human skin," *Nature materials*, vol. 12, no. 10, pp. 938–944, 2013.

[8] D. J. Lipomi, M. Vosgueritchian, B. C. Tee, S. L. Hellstrom, J. A. Lee, C. H. Fox, and Z. Bao, "Skin-like pressure and strain sensors based on transparent elastic films of carbon nanotubes," *Nature nanotechnology*, vol. 6, no. 12, pp. 788–792, 2011.

[9] V. Lumelsky, M. S. Shur, S. Wagner, and M. Ding, "Sensitive skin," 2000.

[10] M. L. Hammock, A. Chortos, B. C.-K. Tee, J. B.-H. Tok, and Z. Bao, "25th anniversary article: the evolution of electronic skin (e-skin): a brief history, design considerations, and recent progress," *Advanced materials*, vol. 25, no. 42, pp. 5997–6038, 2013.

[11] M.-g. Kim, H. Alrowais, and O. Brand, "3d-integrated and multifunctional all-soft physical microsystems based on liquid metal for electronic skin applications," *Advanced Electronic Materials*, vol. 4, no. 2, p. 1700434, 2018.

[12] W. Hu, G. Z. Lum, M. Mastrangeli, and M. Sitti, "Small-scale soft-bodied robot with multimodal locomotion," *Nature*, vol. 554, no. 7690, pp. 81–85, 2018.

[13] S. Gong, W. Schwalb, Y. Wang, Y. Chen, Y. Tang, J. Si, B. Shirinzadeh, and W. Cheng, "A wearable and highly sensitive pressure sensor with ultrathin gold nanowires," *Nature communications*, vol. 5, no. 1, pp. 1–8, 2014.

[14] D. Makarov, M. Melzer, D. Karnaushenko, and O. G. Schmidt, "Shapeable magnetoelectronics," *Applied Physics Reviews*, vol. 3, no. 1, p. 011101, 2016.

[15] R. Geryak and V. V. Tsukruk, "Reconfigurable and actuating structures from soft materials," *Soft matter*, vol. 10, no. 9, pp. 1246–1263, 2014.

[16] D. Romeis, P. Metsch, M. Kästner, and M. Saphiannikova, "Theoretical models for magneto-sensitive elastomers: a comparison between continuum and dipole approaches," *Physical Review E*, vol. 95, no. 4, p. 042501, 2017.

[17] E. COQUELLE and G. BOSSIS, "Magnetostriction and piezoresistivity in elastomers filled with magnetic particles," *Journal of Advanced Science*, vol. 17, no. 1+ 2, pp. 132–138, 2005.

[18] S. Chougale, D. Romeis, and M. Saphiannikova, "Transverse isotropy in magnetoactive elastomers," *Journal of Magnetism and Magnetic Materials*, vol. 523, p. 167597, 2021.

[19] G. Z. Lum, Z. Ye, X. Dong, H. Marvi, O. Erin, W. Hu, and M. Sitti, "Shape-programmable magnetic soft matter," *Proceedings of the National Academy of Sciences*, vol. 113, no. 41, pp. E6007–E6015, 2016.

[20] C. A. Brisbois, M. Tasinkevych, P. Vázquez-Montejo, and M. O. De La Cruz, "Actuation of magnetoelastic membranes in precessing magnetic fields," *Proceedings of the National Academy of Sciences*, vol. 116, no. 7, pp. 2500–2505, 2019.

[21] R. Podgajny, M. Bałanda, M. Sikora, M. Borowiec, L. Spałek, C. Kapusta, and B. Sieklucka, "Cobalt (ii) octacyanotungstate (v) organic–inorganic hybrid ferromagnetic materials with pyrazine and 4, 4-bipyridine," *Dalton Transactions*, no. 23, pp. 2801–2809, 2006.

[22] L. D. Barron, "Chirality and magnetism shake hands," *Nature materials*, vol. 7, no. 9, pp. 691–692, 2008.

[23] J. S. Miller, "Magnetically ordered molecule-based assemblies," *Dalton transactions*, no. 23, pp. 2742–2749, 2006.

[24] J. S. Miller, "Organic-and molecule-based magnets," *Materials Today*, vol. 17, no. 5, pp. 224–235, 2014.

[25] K. V. Yershov, V. P. Kravchuk, D. D. Sheka, J. van den Brink, and Y. Gaididei, "Spontaneous deformation of flexible ferromagnetic ribbons induced by dzyaloshinskii-moriya interaction," *Physical Review B*, vol. 100, no. 14, p. 140407, 2019.

[26] Y. Gaididei, V. P. Kravchuk, and D. D. Sheka, "Curvature effects in thin magnetic shells," *Physical review letters*, vol. 112, no. 25, p. 257203, 2014.

[27] M. I. Sloika, V. P. Kravchuk, D. D. Sheka, and Y. Gaididei, "Curvature induced chirality symmetry breaking in vortex core switching phenomena," *Applied Physics Letters*, vol. 104, no. 25, p. 252403, 2014.

[28] V. L. Carvalho-Santos, R. M. Corona, D. Altbir, and S. Castillo-Sepúlveda, "Shifts in the skyrmion stabilization due to curvature effects in dome-and antidome-shaped surfaces," *Physical Review B*, vol. 102, no. 2, p. 024444, 2020.

[29] V. P. Kravchuk, D. D. Sheka, A. Kákay, O. M. Volkov, U. K. Rößler, J. van den Brink, D. Makarov, and Y. Gaididei, "Multiplet of skyrmion states on a curvilinear defect: Reconfigurable skyrmion lattices," *Physical Review Letters*, vol. 120, no. 6, p. 067201, 2018.

[30] A. Saxena, R. Dandoloff, and T. Lookman, "Deformable curved magnetic surfaces," *Physica A: Statistical Mechanics and its Applications*, vol. 261, no. 1-2, pp. 13–25, 1998.

[31] R. Cacilhas, C. De Araujo, V. Carvalho-Santos, R. Moreno, O. Chubykalo-Fesenko, and D. Altbir, "Controlling domain wall oscillations in bent cylindrical magnetic wires," *Physical Review B*, vol. 101, no. 18, p. 184418, 2020.

[32] G. Bittencourt, R. Moreno, R. Cacilhas, S. Castillo-Sepúlveda, O. Chubykalo-Fesenko, D. Altbir, and V. L. Carvalho-Santos, "Curvature-induced emergence of a second critical field for domain wall dynamics in bent nanostripes," *Applied Physics Letters*, vol. 118, no. 14, p. 142405, 2021.

[33] M. Kuepferling, A. Casiraghi, G. Soares, G. Durin, F. Garcia-Sanchez, L. Chen, C. Back, C. Marrows, S. Tacchi, and G. Carlotti, "Measuring interfacial dzyaloshinskii-moriya interaction in ultra thin films," *arXiv preprint arXiv:2009.11830*, 2020.

[34] G. Gioia and R. D. James, "Micromagnetics of very thin films," *Proceedings of the Royal Society of London. Series A: Mathematical, Physical and Engineering Sciences*, vol. 453, no. 1956, pp. 213–223, 1997.

[35] E. Efrati, E. Sharon, and R. Kupferman, "Elastic theory of unconstrained non-euclidean plates," *Journal of the Mechanics and Physics of Solids*, vol. 57, no. 4, pp. 762–775, 2009.

[36] M. P. Do Carmo, *Differential geometry of curves and surfaces: revised and updated second edition*. Courier Dover Publications, 2016.

[37] K. F. Gauss and P. Pesic, *General investigations of curved surfaces*. Courier Corporation, 2005.

[38] W. C. Young, R. G. Budynas, A. M. Sadegh, *et al.*, *Roark's formulas for stress and strain*, vol. 7. McGraw-hill New York, 2002.

[39] V. H. Carneiro, J. Meireles, and H. Puga, "Auxetic materials—a review," *Materials Science-Poland*, vol. 31, no. 4, pp. 561–571, 2013.

[40] P. Mott and C. Roland, "Limits to poisson's ratio in isotropic materials—general result for arbitrary deformation," *Physica Scripta*, vol. 87, no. 5, p. 055404, 2013.

[41] W. Köster and H. Franz, "Poisson's ratio for metals and alloys," *Metallurgical reviews*, vol. 6, no. 1, pp. 1–56, 1961.

[42] F. Cardarelli, "Materials handbook: a concise desktop reference," 2008.

[43] D. Wagner, *Introduction to the Theory of Magnetism: International Series of Monographs in Natural Philosophy*, vol. 48. Elsevier, 2013.

[44] S. Dasgupta, S. Zhang, I. Bah, and O. Tchernyshyov, "Quantum statistics of vortices from a dual theory of the x y ferromagnet," *Physical Review Letters*, vol. 124, no. 15, p. 157203, 2020.

[45] M. Bryan, J. Dean, and D. Allwood, "Dynamics of stress-induced domain wall motion," *Physical Review B*, vol. 85, no. 14, p. 144411, 2012.

[46] P. S. Vilas-Boas, R. G. Elias, D. Altbir, J. M. Fonseca, and V. L. Carvalho-Santos, "Topological magnetic solitons on a paraboloidal shell," *Physics Letters A*, vol. 379, no. 1-2, pp. 47–53, 2015.